Tubing qualities for extremely high corrosive environments

Master Thesis

Montanuniversität Leoben

In cooperation with

OMV Laboratories, Gänserndorf

Author: **Georg Stechauner**

Industry Advisor: **Dr. Gerald Zehethofer**
Senior Corrosion Engineer

University Advisor: **Assoc. Prof. Dr. Gregor Mori**

To my parents

for supporting me in every step I made

To my brother

for being my best friend

And my dearest one

for showing me, that love is the greatest good

“Persönlichkeiten werden nicht durch schöne Reden geformt, sondern durch Arbeit und eigene Leistung.“

[Albert Einstein]

„Strebe nach Ruhe, aber durch das Gleichgewicht, nicht durch den Stillstand deiner Tätigkeit.“

[Friedrich Schiller]

Eidesstattliche Erklärung

Ich erkläre hiermit an Eides statt, dass die vorliegende Diplomarbeit

Tubing qualities for extremely high corrosive environments

von mir selbst und nur unter Verwendung der angeführten Literatur verfasst wurde.

Georg Stechauner, Leoben im Februar 2011

Table of Contents

Acknowledgements

I want to thank my advisors for their support and counselling received over the course of this thesis. Their ideas, input and experience were a great help and inspiration for me.

Furthermore, I would like to express my gratitude to Dr. Hönig whose understanding and skill truly enhanced the quality of my work.

Great thanks go to Dr. Zehethofer and Dr. Havlik, for making this work possible, and supporting me, whenever help was needed.

Special thanks go out to Mr. Franz Hellmer and Mr. Robert Arzt, who were supporting me in the laboratories and enabling me to be successful with the experimental part.

I especially want to thank Professor Mori, for his great skill in explaining problems and solving them, as well as his guidance.

I want to recognize Dr. Gumpendorfer, for explaining the art of statistics to me, as well as Mr. Leopold Steinmayer, whose help in crafting the corrosion samples was of immeasurable value.

Last but not least, I would like to thank the facility staff, for supplying me with my daily breakfast, as well as cleaning the instruments of my experiments.

1 Abstract

The importance of chemical composition and microstructure on carbon dioxide corrosion of carbon and low alloy steels is generally recognized, however certain aspects are still uncertain as to what degree the parameters influence the corrosion. Moreover contradictory results can be found in literature. As chemical composition and microstructure are not independent variables, the same microstructure can be seen for different chemical compositions and vice versa. Many authors use different parameters such as temperature, immersion time, testing method and so on, and it is therefore almost impossible to compare them directly.

As a consequence of this actual situation, OMV wanted to investigate the behavior of selected steel grades at certain parameters, which were of the companies' interest. The aim of this work is to find the best steel fitting for the chosen parameters and to compare them to the literature in order to clarify this topic. The results shall be used for further tests, in order to see in which fields work still has to be done, and to be a basis for the engineers in choosing the right material.

This work starts with a literature review, which will present the reader the state-of-the-art on the topics of CO_2 corrosion basics and environmental influences, as well as the influence of chemical composition and microstructure. In the next chapter the sample treatment, used testing methods, mass loss and electrochemical measurement, as well as the statistical evaluation will be described. The next section presents the results of all the conducted tests which will be discussed in the following section. On the last pages, a conclusion will be drawn of the experiments and an outlook on the topic will be given.

It was shown that the carbon steels performed better for the used environments than low alloyed steels with chromium. A great influence on the variance of the results was found to be within the amount of used medium. Generally a higher corrosion rate was found for short testing times. Only a small influence of the microstructure on the corrosion rate was found.

2 CO_2 corrosion of steels

2.1 Basics of CO_2 corrosion

CO_2 corrosion is and has been a severe problem throughout the age of petroleum production. However, the attention of the engineers was directed towards this problem for the first time in the mid-forties of the 20th century when CO_2 corrosion problems appeared in Texan wells [1]. Since then, the basic reactions have been studied under laboratory and field conditions, and several models for the calculation of the expected corrosion rate have been developed. Still it is not possible, to reliably predict the corrosion rate for high pressures, or other parameters such as temperature, microstructure or chemical composition. The influences of how these environmental factors affect the film formation and thus the CO2 corrosion are covered in the following chapters.

2.1.1 Basic reactions of CO_2 corrosion

When CO_2 is present in the gas phase, any water in contact with it will dissolve it up to a concentration which is proportional to the partial pressure, p_{CO2}, of the CO_2 in the gas following Henry's law [2]:

$$p_{CO_2} = K * x_{CO_2} \quad (1)$$

$$p_{CO_2} = (mole\%\, CO_2) * (gas\ pressure) \quad (2)$$

where p_{CO2} is the partial pressure of carbon dioxide in the bulk atmosphere [Pa], K is Henry's constant in [Pa] and x_{CO2} is the equilibrium mole fraction of solute in liquid phase [-].

After dissolving, the gas forms carbonic acid in the water [3]:

$$CO_2 + H_2O \longrightarrow H_2CO_3 \quad (3)$$

For the corrosion of carbon steel in CO_2 containing solutions several mechanisms have been suggested. The main reactions can be described by three cathodic and one anodic reaction [4; 5]. While equation (4a) is predominant at low pH-values, equations (4b) [4] and (4c) [5] become overly important as the pH increases [6]. Reaction (5) shows the dissolution of metallic iron into ionic iron:

$$2H^+ + 2e^- \longrightarrow H_2 \quad (4a)$$

$$2HCO_3^- + 2e^- \longrightarrow 2CO_3^- + H_2 \quad (4b)$$

$$2H_2CO_3 + 2e^- \longrightarrow 2HCO_3^- + H_2 \quad (4c)$$

$$Fe \longrightarrow Fe^{2+} + 2e^{-} \quad (5)$$

Due to the dissolution of iron and the presence of carbonates, a corrosion layer can be formed on the steel surface. The existence of this very layer has an important influence on the corrosion rate and has to be taken into account when studying the corrosion of steels in aqueous, CO_2 environments. The formation of the iron carbonate, $FeCO_3$, can be explained via two routes using equations (6) and (7a,b) respectively:

$$Fe^{2+} + CO_3^{2-} \longrightarrow FeCO_3 \quad (6)$$

$$Fe^{2+} + 2HCO_3^{-} \longrightarrow Fe(HCO_3)_2 \quad (7a)$$

$$Fe(HCO_3)_2 \longrightarrow FeCO_3 + CO_2 + H_2O \quad (7b)$$

Even though carbonic acid is a weak acid and only a small fracture of it dissociates, it can be more corrosive than a completely dissociated acid at the same concentration [7].

$$HCO_3^{-} + H^{+} \longleftrightarrow H_2CO_3 \quad (8)$$

Using equations (4c) and (8) it can be explained, why carbonic acid can be more corrosive than a completely dissociated acid at the same concentration. For one reason, the lower pH, due to the carbonic acid, increases the rate of iron dissolution. The other reason lies within the catalyzing effect of the undissolved carbonic acid which promotes the hydrogen evolution reaction.

2.1.2 Film Formation

The existence of a maximum corrosion rate indicates that a superposition of two controversial processes exist [8]. At lower temperatures, on a steel with no scale, the corrosion rate increases with increasing temperature, as the process is controlled by surface reactions. Further, the formation of the Fe_3C layer can increase the corrosion rate. The second process is controlled by the formation of $FeCO_3$, which decreases the corrosion rate, as the mass transfer of iron or bicarbonate ions becomes the rate determining step [8].

The compiled information gathered by many authors shows four classes of corrosion films, in the range from 5°C to 150°C:

- Transparent films
- Ferrous carbide films (Fe_3C)
- Ferrous carbonate films ($FeCO_3$)
- Combined Fe_3C and $FeCO_3$ films

Transparent films – are encountered at low temperatures (<20°C) and are less than 1µm thick. This film is thermodynamically not the most stable film that can form, however it needs no carbonate and only very little ferrous ion concentration. Auger electron spectroscopy showed a ratio of iron to oxygen ions in the proportion of about 1:2. The authors educe that this film could consist of FeOOH and showed that it reduced the corrosion rate [9].

Ferrous carbide (Fe_3C) films – develop upon the anodic dissolution of ferrite phase in carbon steels, leaving the cathodic Fe_3C behind. These films significantly affect the corrosion process and increase the corrosion rate by a few times [10]. The processes are as following:

- As cementite (Fe_3C) is cathodic, a galvanic couple forms, which can accelerate the dissolution of iron [10].
- As cathodic reactions take place preferentially at the cathodic Fe_3C sites, the corrosion process gets physically separated into cathodic and anodic sites. This separation leads to a change in the pH of the medium, as the solution in contact with the cathodic site becomes more alkaline, and the solution at the anodic site becomes acidic. This local acidification can promote increased corrosion rates [1; 10].
- The carbide lamellae provide local flow stagnation, which can lead to increased Fe^{2+} concentration. Hence supersaturation of Fe^{2+} is reached faster and $FeCO_3$ can precipitate [11].
- If the conditions lead to the combined occurrence of Fe_3C and $FeCO_3$, the cementite can act as a framework for the ferrous carbonate to anchor. This improves the tolerance to mechanical forces and reduces the corrosion rate [11].

Ferrous carbonate ($FeCO_3$) films – take the most important role at reducing corrosion effects on carbon steels in CO_2 environments. The precipitation is highly dependent on temperature, flow, microstructure, and the supersaturation of the medium with $FeCO_3$. There is an agreement among all authors, that an increased temperature improves the protectiveness and adherence [12] of the $FeCO_3$ scale, but no common value for the optimal temperature is known. In some environments the maximum corrosion rate was measured at 60°C to 70°C [12], whereas others measured the peak to be at higher temperatures of 90°C [13] or lower temperatures of 50°C [9]. More on the influence of temperature will be covered in chapter 2.1.3.

Combined Fe_3C and $FeCO_3$ films – are the most common films found on carbon steels in sweet environments. As the ferrite corrodes away, the Fe_3C is left behind as it is cathodic, thus corrosion resistant. Depending on where and how the $FeCO_3$ precipitates, determines if the scale is protective, or not. This topic was described by Crolet et al. [10] and will be covered in chapter 2.3.

2.1.3 Influence of environmental factors

It is important to mention that scale formation, and thus corrosion rate, is not solely dependent on a single parameter, but on an array of factors including temperature, partial pressure CO_2, flow, acidity and other environmental and metallurgical effects.

pH

An increase in pH decreases the corrosion rate (Figure 1), if temperature and CO_2 pressure are kept constant. At a constant volume, the Fe^{2+} concentration will increase during the experiment while the H^+ concentration decreases with time, until the solution is saturated with $FeCO_3$. When saturated, the pH of the solution will not change anymore with the addition of Fe^{2+}. In the early stages, the corrosion rate often changes with time, but passes through a plateau, a broad maximum or a steady-state region [7; 14]. Because of this change, "fresh", Fe-ion free water can induce much higher corrosion rates than predicted by certain models and nomograms [7].

pH is one of the most important factors for the $FeCO_3$ film formation. An increase in the pH, lowers the solubility of $FeCO_3$ in the medium, hence precipitation is promoted and the corrosion rate is lowered [15]. Videm et al. [9] showed that at an increased pH, even at low temperatures, a $FeCO_3$ film can form and reduce the corrosion rate (Figure 1).

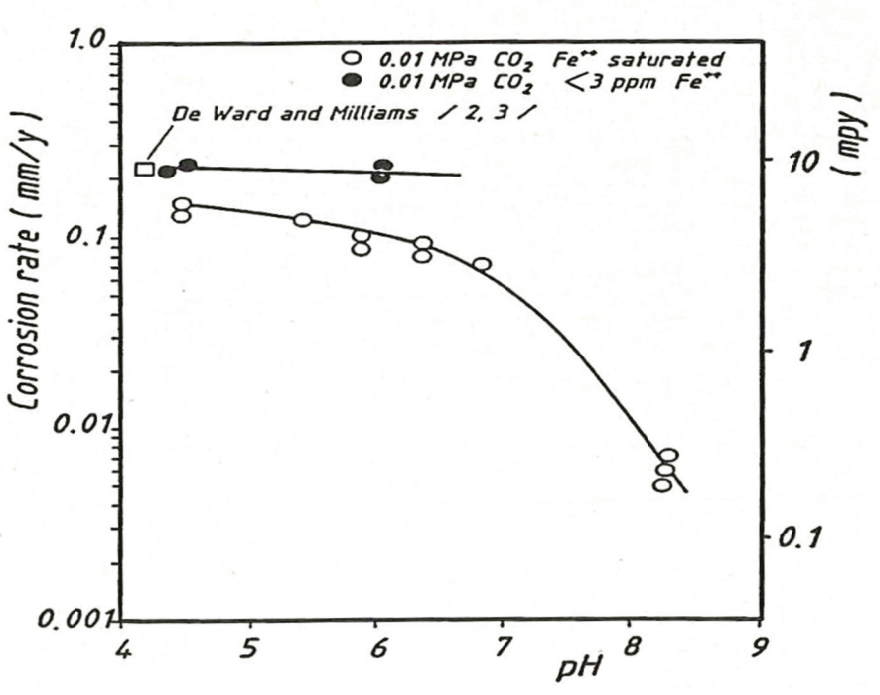

Figure 1 – Corrosion rate as a function of pH at 0.1 bar CO_2 partial pressure. 3.5% NaCl, 20°C, unalloyed carbon steel [9].

Iron content

The amount of iron cations in the solution determines whether a passive $FeCO_3$ film will be formed or not. Therefore low concentrations of Fe^{2+} and high CO_2 levels can lead to rapid corrosion [16]. When the solubility limit of Fe^{2+} in the brine is reached, $FeCO_3$ tends to form. This carbonate can build a scale on the sample, lowering the corrosion rate. Figure 2 shows the corrosion rate of steel in 3.5% NaCl brine at 20°C at different CO_2 partial pressures as a function of temperature.

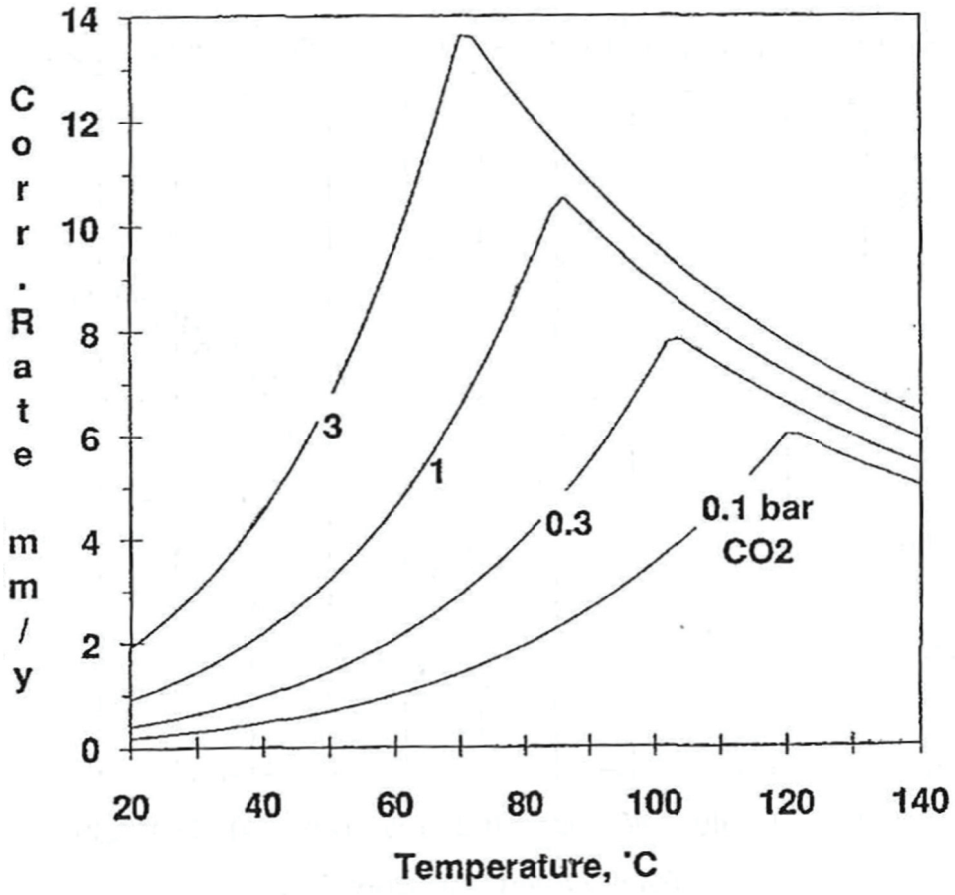

Figure 2 – Corrosion rate as a function of temperature and pressure according to deWaard-Milliams equation incorporating the scale factor [14].

CO_2 partial pressure

The concentration of the carbonic acid is proportional to the carbon dioxide partial pressure. The amount of CO_2 that can be dissolved in the brine can be calculated using Henry's law or other models. Duan and Sun presented a model [17] for calculating the solubility of CO_2 in water and aqueous NaCl solutions from 273 to 533K and from 0 to 2000 bar.

The higher the partial pressure of CO2 the lower the pH. As shown in Figure 3, the change in pH in condensed water saturated with Fe^{2+} from 0 to 5 bar is from 7.1 to 4.6, whereas the change from 5 to 50 bar is only from 4.6 to 4.0. Many authors [7; 14; 18; 19; 20] developed models to

predict the corrosion rate based on a partial pressure of a few bar. No models are existent on the effect of higher pressures going up to 30 bar or more.

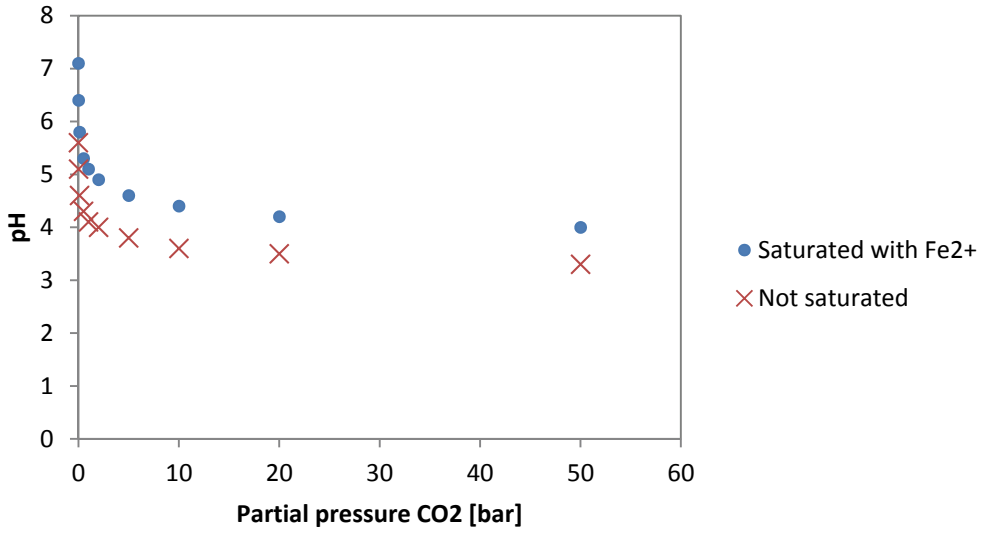

Figure 3 – pH as a function of partial pressure calculated with NORSOK formula at 80°C.

However, the change in pH is by no means the only effect of carbon dioxide partial pressure on the corrosion behavior of the samples. Hesjevik et al. [21] show in their work the corrosion rates of low alloy carbon steels exposed to water at very high CO_2 pressures (up to 95 bar). The highest corrosion rate was achieved at 58 bar, decreasing to both sides. The lowest corrosion rate was achieved at 95 bar. The authors could not explain their results with present CO_2 corrosion models, as those models are firstly not made for such high pressures, and secondly show increased corrosion rates with increased pressure. Moreover, they measured almost no difference in the corrosion rate for two different pH values in a separate test row. A similar observation was reported by M. Seiersten [22]. Corrosion rates decreased steadily from 5.6 mm/y at 10 bar to 0.6 mm/y at 95 bar.

On the lower end of the pressure scale (1-7 bar), Videm et al. [16] reported that the corrosion rate increases proportionally with the CO_2 partial pressure to a power of about 0.7.

Hesjevik et al. [21] propose that different corrosion mechanisms are at work at the tested high pressures, compared to the lower pressures where the existing models are valid. Therefore the models cannot be used in the high pressure regime. They could not find a definite cause, so more work needs to be done in order to understand the corrosion mechanisms that take place in this pressure range.

Temperature

The operating temperature strongly affects the characteristics and morphology of surface film, which, in turn, influences the CO_2 corrosion process. DeWaard and Milliams [4] showed that the corrosion rate of grit-blasted samples increases, as the temperature increases up to a certain temperature where a maximum in the corrosion rate is reached. They experienced that at temperatures above 80°C the samples were always covered with a black, protective layer, resulting in a decreased corrosion rate. This was also shown by Nesic and Lunde [23]. This happens because the solubility of $FeCO_3$ in the solution decreases and a state of supersaturation is reached faster. This leads to $FeCO_3$ precipitation, hence to the formation of a possibly protective film [12; 15]. They also revealed that at low temperatures of 20°C it was difficult to form protective layers, even when the $FeCO_3$ concentration exceeded the thermodynamic saturation limit.

Moreover the adherence and hardness of a film correlates with the temperature of the system [9]. While layers below 40°C could be removed by wiping with a cloth, they were adherent at 60°C. At temperatures ranging from 90-150°C the scale was so enduring that it couldn't be scraped off with a plastic knife.

For lower temperatures of about 40°C the corrosion rate increases with temperature, due to the high solubility of $FeCO_3$ and the elevating reaction and diffusion speeds.

Controversial results were shown by Yin et al. [24] who were investigating the effect of temperature on the corrosion product layer of carbon steel exposed to CO_2 containing solutions. By the means of scanning electron microscopy with energy dispersive spectrometry, X-ray diffraction and X-ray photoelectron spectroscopy they characterized the morphology and composition of the layer and the corrosion rate by the means of weight loss measurements. The thicknesses of the corrosion product layers were measured to decrease with increasing temperature. However, weight loss methods showed that the thickness of the layer does not provide increased corrosion resistance, rather the opposite. The authors presented a corrosion rate maximum at 50°C which decreased at higher temperatures.

2.1.4 Models for prediction of CO_2 corrosion

In order to save time, materials and efforts, it has become common to simulate and model processes of technical interest. In the case of CO_2 corrosion, the first model for the prediction of corrosion of carbon steels was created by deWaard and Milliams [4], hence the formula for calculating the corrosion rate is often referred to as the deWaard-Milliams equation [14] (9).

$$\log(V_{cor}) = 5.8 - \frac{1710}{273 + T} + 0.67 \log(p_{CO_2}) \quad (9)$$

where V_{cor} is the corrosion rate [mm/y], T is the temperature [°C] and p_{CO2} is the partial pressure of CO_2 [bar]. The dependence of the corrosion rate on temperature and partial pressure and the influence of scale formation can easily be read from the following nomogram:

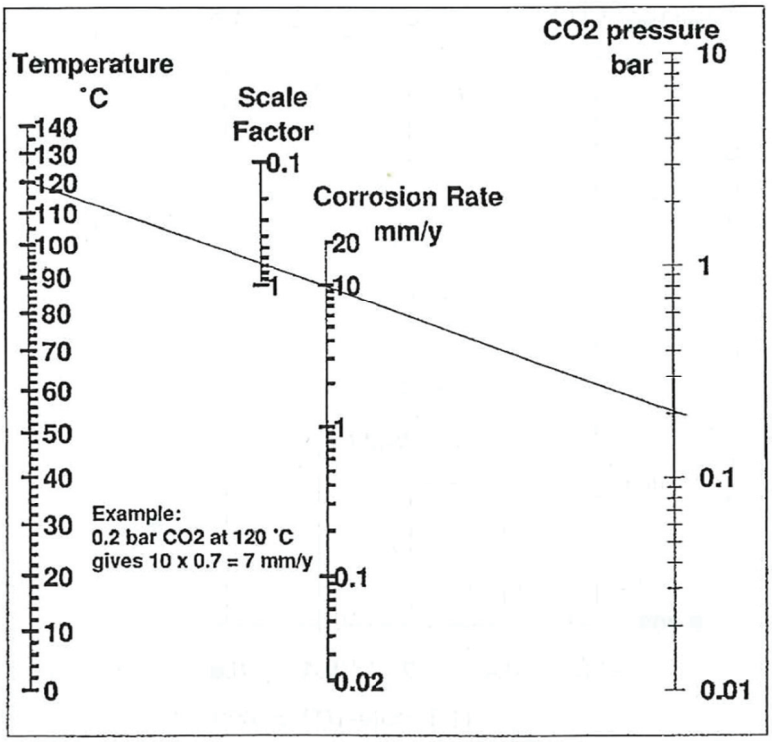

Figure 4 – Nomogram for CO_2 corrosion using deWaard-Milliams equation [14].

The corrosion rate read from this figure can be seen as a worst case scenario, because reaction (9) would imply that there are no reaction limitations from mass transfer effects. Moreover there are many correction factors which have to be applied to this formula in order to achieve an adequate result such as the effect of corrosion product films, the influence of pH, the effect of flow velocity, or the effect of Glycol or Methanol. The corrosion rate tends to decrease to zero for temperatures exceeding the scaling temperature, at which scale formation begins. The scaling factor applied in the nomogram is a conservative, minimum protection factor.

Another model (10) for the calculation of the corrosion rate of CO_2 corrosion is the NORSOK Standard model [20]. "The model is an empirical corrosion rate model for carbon steel in water containing CO_2 at different temperatures, pHs, CO_2 fugacities, and wall shear stresses. It is based on flow-loop experiments at temperatures from 5°C to 160°C" [20].

$$CR_t = K_t * f_{CO_2}^{0.62} * (S/19)^{0.146+0.0324\log(f_{CO_2})} * f(pH)_t \quad (10a)$$

$$CR_t = K_t * f_{CO_2}^{0.36} * (S/19)^{0.146+0.0324\log(f_{CO_2})} * f(pH)_t \quad (10b)$$

$$CR_t = K_t * f_{CO_2}^{0.36} * f(pH)_t \quad (10c)$$

where CR_t is the corrosion rate at temperature t [°C], K_t is a tabulated constant for temperature t, f_{CO2} is the fugacity of CO_2 [bar], S is the wall shear stress [Pa] and $f(pH)_t$ is the pH factor at temperature t. The validity of the equations is as following:

- *10a:* 20°C to 150°C
- *10b:* 15°C
- *10c:* 5°C.

The model developed by Nesic et al. [18] is based on modeling individual electrochemical reactions in a water-CO_2 system. It shows the same trend as the other models for pressures p_{CO2} > 1 bar, but a different one for pressures below one bar. Nesic et al. reported that at these low pressures the H^+ reduction dominated, whereas deWaard et al. and NORSOK simply extrapolated their values. The authors close that their model gives a clearer picture of the corrosion mechanisms and the effect of key parameters. A model, similar to this one was developed by Mishra et al. [19]. Just like the model of Nesic, this one is based on chemical reaction-controlled processes which are applicable as long as no scale formation begins. The model has a similar form as the others and the results of it agree with them.

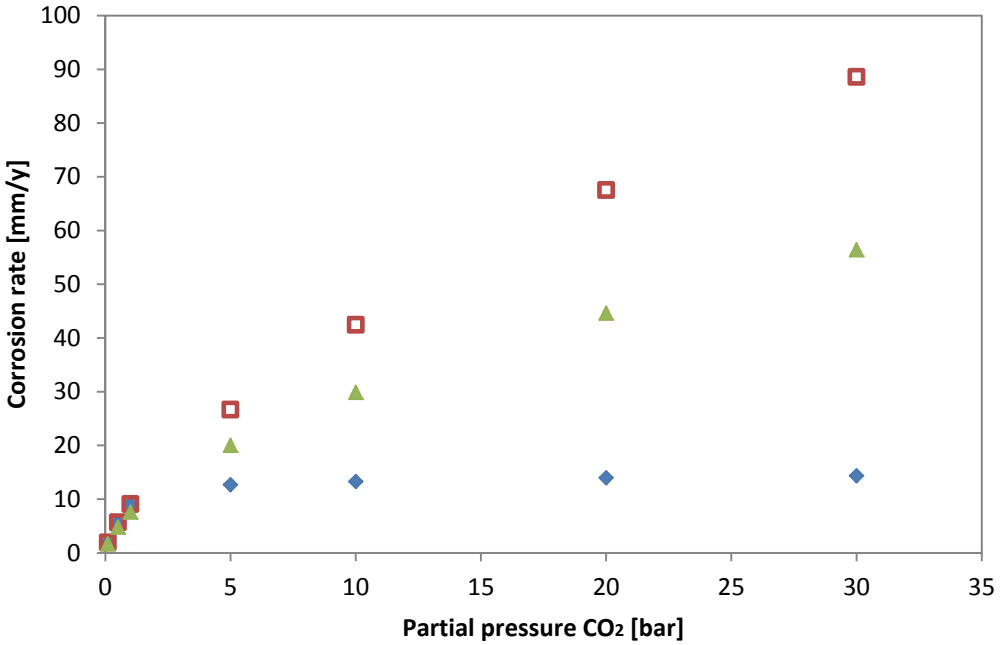

Figure 5 – Comparison of deWaard-Milliams and NORSOK model. Blue diamonds represent deWaard-Milliams with scaling factor, red squares without scaling factor. Green triangles represent NORSOK.

As Figure 5 shows, the scaling factor has a huge impact on the calculated corrosion rate. Its determination is of utmost importance, to calculate an accurate corrosion rate. However as the following chapters will show, this is not an easy task, as the scale formation is dependent on so many parameters, that a general answer is next to impossible.

2.2 Influence of chemical composition

Apart from the environmental factors described above, chemical composition of steel is a key factor influencing the CO_2 corrosion. Thus understanding the influences of the alloying elements and their range of effectiveness in decreasing the corrosion rates is of utmost importance.

Figure 6 is a schematic presentation of the relative effect of microalloying elements on the corrosion rate. The elements will be discussed in detail in the following chapter.

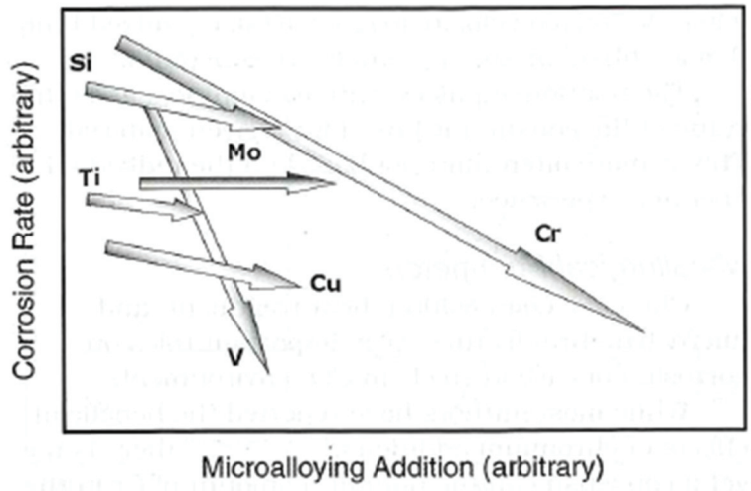

Figure 6 – Schematic presentation of relative effect of additional microalloying elements on corrosion rate [15].

2.2.1 Chromium

Out of all alloying elements for C-Steels used in the oil and gas industry, chromium was paid the greatest attention by far, and is therefore the main element which comes to mind for the reduction of corrosion. It is generally known that the addition of 13%Cr or more reduces corrosion due to passivation and was shown by various authors [25; 26]. This great deal of interest was amplified by many publications which showed beneficial effects of chromium on the CO_2 corrosion resistance when alloying only a few percent [27; 28; 29; 30; 31; 32]. On the other hand, there are only a handful of authors, which describe unfavorable effects upon the addition of chromium [33; 34]. In a few cases the effectiveness of chromium is highly dependent on factors like immersion time, chloride concentration or temperature [13; 33] or the effect is unclear [35].

For an easier reading, the parameters of testing and the results, if the application of chromium had a beneficial impact upon the corrosion rate, are summarized in Table 1. This table shows

that except Dugstad et al. [31] and Schmitt et al. [34] all others report a beneficial effect of chromium at low pressures. Those authors investigated the behavior of chromium free C-Steels up to 13%Cr steel grades. The flow velocity was also a topic and provides some important results.

Ikeda et al. [13] performed a thorough study on this topic and systematically examined the corrosion behavior of Cr-containing steels. They measured the dependence of the corrosion rate on the temperature for different chromium alloys and showed that the corrosion rate has a peak value, which moves to higher temperature for higher chromium amounts. Figure 7 shows that for constant parameters and a changing temperature, the corrosion rate of the chromium alloys varies greatly. The nature of the peak was described in the previous chapter, the shift of the peak with increasing chromium amounts is explained with the suppression of iron dissolution due to $Cr(OH)_3$ formation [13]. Thus it needs a higher temperature to reach supersaturation of Fe^{2+} ions which is a necessity for the formation of $FeCO_3$. The authors describe the formation of $FeCO_3$ as unfavorable in the case of chromium alloy steels, as the co-deposition of $Cr(OH)_3$ and $FeCO_3$ leads to concurring growth of the scales and therefore an increased corrosion rate. At low partial pressures of CO_2 the suppression of dissolution is even more effective. This will be shown later by other authors who performed their tests in a pressure range of 1-2 bar.

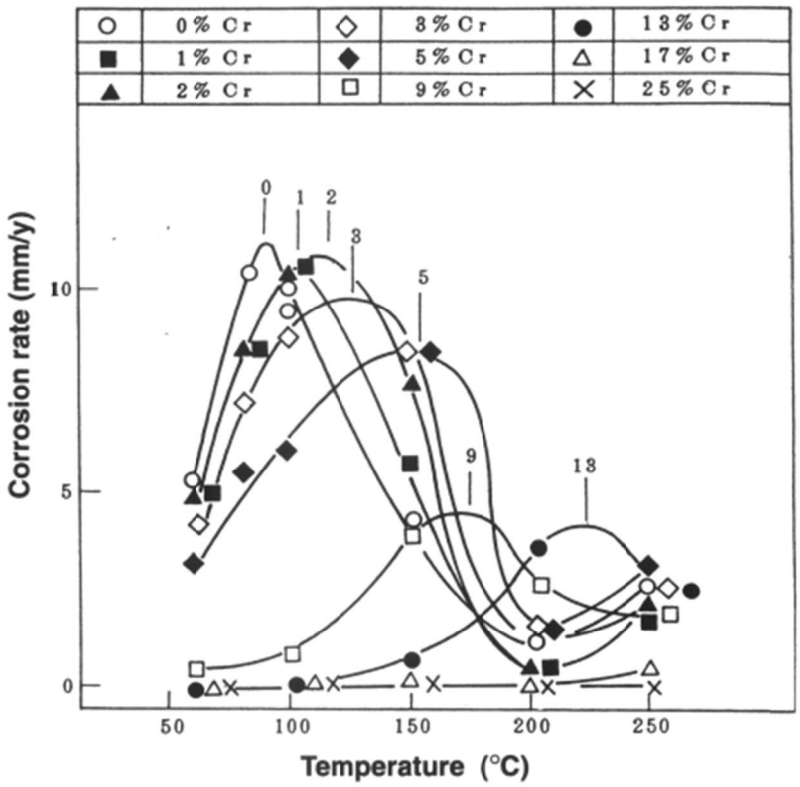

Figure 7 – Corrosion rate as a function of temperature and chromium content on CO_2 corrosion of iron-chromium alloys. Autoclave testing, p_{CO2} 30 bar, 5% NaCl, 96 hours exposure time, 2.5 m/s flow velocity, 25 ml/cm^2 specific volume [13].

Table 1 – Parameters of analysed literature and the effectiveness of chromium. Ref: Reference; Temp: Temperature; p_{CO2}: partial pressure CO_2; Ratio M/S: Ratio between volume of medium and surface area. Effect: ++: beneficial effect, +-: unclear or dependent on other parameters, --: unfavourable effects. Slash "/" represents values not mentioned in literature.

Author	Ref.	Temp. [°C]	p_{CO2} [bar]	Ratio M/S [ml/cm²]	Time [h]	Medium	Flow [m/s]	Effect
Lotz	(25)	60	3	/	50	3% NaCl	2	++
Pfennig	(26)	60	60	/	8000	NaCl	0	++
Kermani	(27)	50-120	1	>20	360	10% NaCl	3	++
	(27)	80	1	>20	/	10% NaCl	0	++
Muraki	(28)	80	1	>20	96	5% NaCl	1	++
Inaba	(29)	30-90	1	/	>170	0.1% NaCl	1	++
Carvalho	(30)	23	1	>20	12-72	11% NaCl	0	++
Dugstad	(31)	60	2	>20	>240	/	3.1-13	++
	(31)	60	2	>20	>240	/	0.1	--
Edmonds	(32)	50	1	>20	336	1% NaCl	/	++
Bosch	(35)	40-90	1 & 30	>20	336	0.1% NaCl	1	+-
Ikeda	(13)	50-200	30	>20	96	5% NaCl	2.5	+-
OMV Report	(33)	60	40	0.6	168	5% NaCl	0	+-
	(33)	100	40	0.6	168	5% NaCl	0	--
	(33)	20	15	/	2 months	16000 ppm Cl^-	/	--
Schmitt	(34)	25	1	/	25-500	7% Na_2SO_4	/	--

Another impact on the corrosion rate is found at the concentration of chlorides. Figure 8 shows that during the first 100 hours, the corrosion rate of a high chromium alloy (chloride concentrations greater than 30000ppm) is higher, than for a low alloy steel grade. After this initial period the higher alloyed steel grade passivates, whereas the formation of the Cr-hydrated protective film of the other grade is disturbed by the Cl^- ions and does not. At lower chloride concentrations of 100ppm, both steel grades perform similar and begin to passivate after 100 hours.

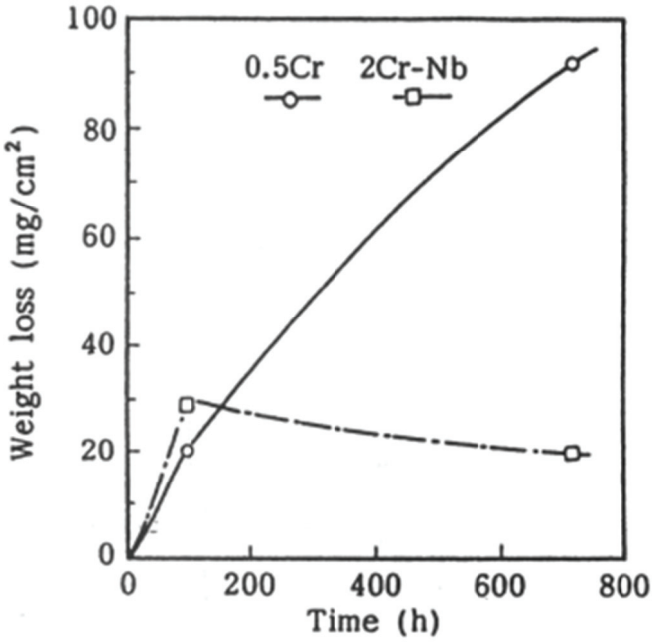

Figure 8 – Weight loss as a function of time and chromium content on CO_2 corrosion of chromium linepipe steels. Loop test, p_{CO2} 1 bar, 5% NaCl, temperature 60°C, 96 and 720 hours exposure time, 2.5 m/s flow velocity, 800 ml/cm² specific volume [13].

The data of other authors who performed their tests at high pressure is either unclear [35] or shows an unfavorable effect of alloying chromium [33]. Bosch et al. [35] performed an immersion test at the shown parameters, and achieved similar corrosion rates for all used steel grades ranging from 0.5%Cr to 1%Cr. They concluded that a variation of chromium contents in this range does not decisively improve the corrosion resistance. An internal report of OMV by Oberndorfer et al. [33] shows that the addition of 1%Cr can dramatically worsen the corrosion resistance of the steel alloy. By the use of an autoclave immersion test as well as a field test, various steel grades, containing chromium amounts of 0 and 1%Cr as well as a 13%Cr steel, were tested. The results of the laboratory autoclave test show that temperature is an important influence factor. The differences in the corrosion rates of the unalloyed and low alloyed grades increase from around 15% to almost 600% after increasing the temperature from 60°C to 100°C. A similar result was achieved from the field test, were the low alloyed steel grade always showed higher corrosion rates than the unalloyed. It has to be mentioned, that as soon as H_2S is introduced to the corrosion system, the 1%Cr steel grade outperforms the unalloyed. The 13%Cr steel grade was used to verify the testing measurement, and showed as expected the lowest corrosion rate throughout all tests.

Schmitt et al. [34] show a critical increase in the corrosion rate of C-Steels when alloying chromium. They performed immersion tests with stirred disc specimen. The investigated materials consisted of C-Steels with varying amounts of chemical elements like carbon or chromium. In contrast to the other authors, a Na_2SO_4 solution was used compared to the NaCl solution. It is therefore questionable if the results can be compared directly to the others. Still, a

corrosion rate up to 15 times higher was measured for chromium alloyed steel grades, compared to an unalloyed C-Steel at parameters, where other authors measured a beneficial effect of chromium.

The change of protectiveness of chromium in dependence of flow rate which was shown in Table 1 by Dugstad, can also be seen in Figure 9. While for high flow rates the corrosion rate decreases with an increase of chromium content, the beneficial effect of chromium is lost for low flow rates.

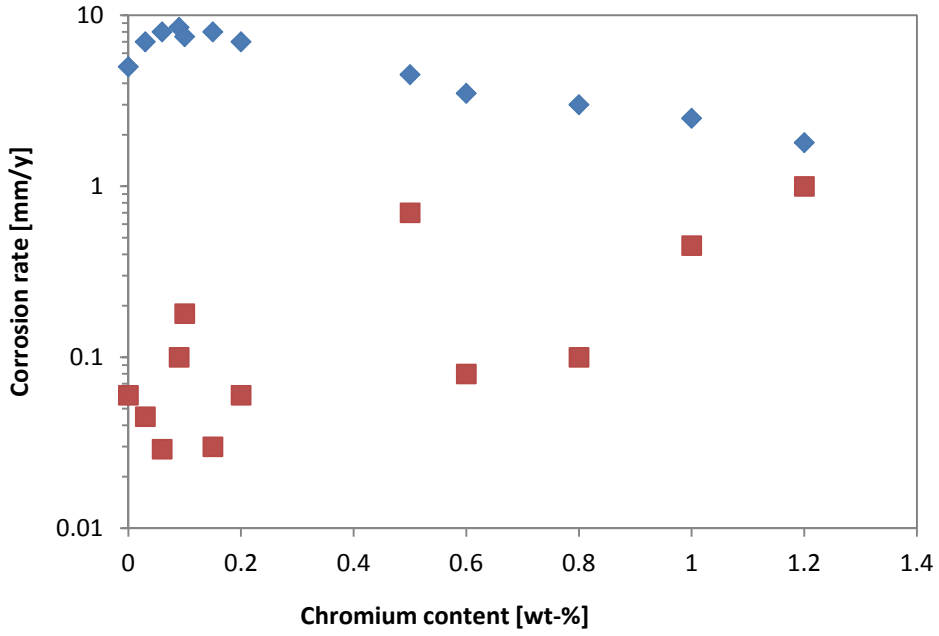

Figure 9 – Corrosion rate as a function of chromium content in steel. Steels were exposed to 60°C and 0.2 MPa CO_2 partial pressure. Blue diamonds were exposed to 350 Pa shear stress, red squares to 0.2 Pa respectively [31].

Still, a great deal of authors report the beneficial effect of chromium on the corrosion rate. As Table 1 shows all of those tests were performed at relatively similar parameters, hence it is reasonable that most of them show the same results. All the authors who reported beneficial effects of chromium held their experiments at low partial pressures of CO_2 of no more than 5 bar. Due to this low pressure the dissolution of iron gets suppressed as stated above. Inaba et al. [29] explain the reduced corrosion rate by the decrease in the stable region of Fe^{2+} in the electrochemical potential diagram by the formation of the oxide layer $Fe_xCr_{3-x}O_4$. Carvalho et al. [30] investigated steels with chromium contents ranging from zero to five percent. They reported that the corrosion rate decreases as the amount of chromium increases. This effect was measured for pH 4.2 and 5.0, but was not measured for pH 6.0. Similar results were reported by [27; 28; 31; 32], and all of them reported the formation of a dense and protective layer due to the chromium.

2.2.2 Carbon

There is very little literature dedicated solely on the effect of carbon on the corrosion rate. As most authors study the influence of chromium, steel grades with small amounts of carbon are used. More often the influence of carbon content was investigated in connection with the microstructure which was formed. This effect will be discussed in the following chapter.

Guo et al [36] investigated the influence of carbon content and microstructure on the corrosion behavior of weathering steels. Three different steel grades with varying carbon content were tested. In the first test, Steel C (0.08 wt-% C) showed a higher corrosion rate than Steel A (0.0036 wt-% C) and Steel B (0.10 wt-% C). However in the second test, Steel A had the highest corrosion rate whereas B and C performed equally well. They concluded that the corrosion behavior of the same steel can be absolutely different in different environments. It is not possible to infer the corrosion rate, by solely knowing the carbon content of a sample, without knowing the microstructure which is formed.

Al-Hassan et al. [37] compared a pure ferrite with no carbon at all versus an eutectoid pearlite steel grade. At all temperatures, the corrosion rate of the pure ferrite was about 5 times lower than the eutectoid pearlite. The result is understandable as the cementite in the pearlite phase is seen to be cathodic. However it is hard to transfer this finding onto any other experiment, as there is always carbon in technical materials, for mechanical reasons. Moreover is the amount of pearlite phase not solely dependent on carbon, but also other elements as well as the thermomechanical history.

2.2.3 Others

Apart from chromium, the influence of other chemical elements was mostly determined at alloy fine tunings, where in almost every case, chromium was present as well [15; 28; 31; 32]. Therefore it is hard to differentiate between a combined effect of the element with chromium and its own effect on the corrosion behavior of the steel/system combination. Schmitt et al. presented results in his work of steel grades with elevated amounts of copper and phosphor and very little chromium [34]. Parameters of cited literature according to Table 1.

Vanadium

For chromium to be effective it is necessary that it is free in the matrix, and not combined with carbon building precipitations. Kermani et al. [27] investigated the effect of the addition of strong carbide-forming elements like V, Ti and Nb. A great percentage of vanadium builds carbides, so the chromium was measured in all samples to be at the level of addition. This was responsible for a major effect on reducing the corrosion rate. This beneficial effect has also been reported by Edmonds et al. [32].

Titanium

Beneficial effects were reported, but the mechanical properties were more variable and difficult to control [32].

Silicon

Dugstad et al. [31] could not find a clear answer on whether silicon has a beneficial effect or not, as the composition was not independent of other elements. Edmonds et al. [32] report enhanced Si to be beneficial. Stegmann et al. [8] attributed higher corrosion resistance to silicon. They postulated that silicon stays on the surface during corrosion, increasing the sticking coefficient which promotes the formation of $FeCO_3$.

Copper

Dugstad and Edmonds reported the same behavior for copper as they did for silicon, however Schmitt et al. [34] report a detrimental effect. The steel grades had elevated amounts of copper with the other elements being in range of the unalloyed steels. Black, loose corrosion products which contained substantial amounts of copper were detected, and high corrosion rates were measured. Kermani et al. [27] report copper being beneficial complementary to chromium and vanadium. Stegmann et al. [8] also report a beneficial corrosion behavior of a N80 steel grade with 0.19 wt-% copper compared to a N80 steel grade with 0.01 wt-% copper.

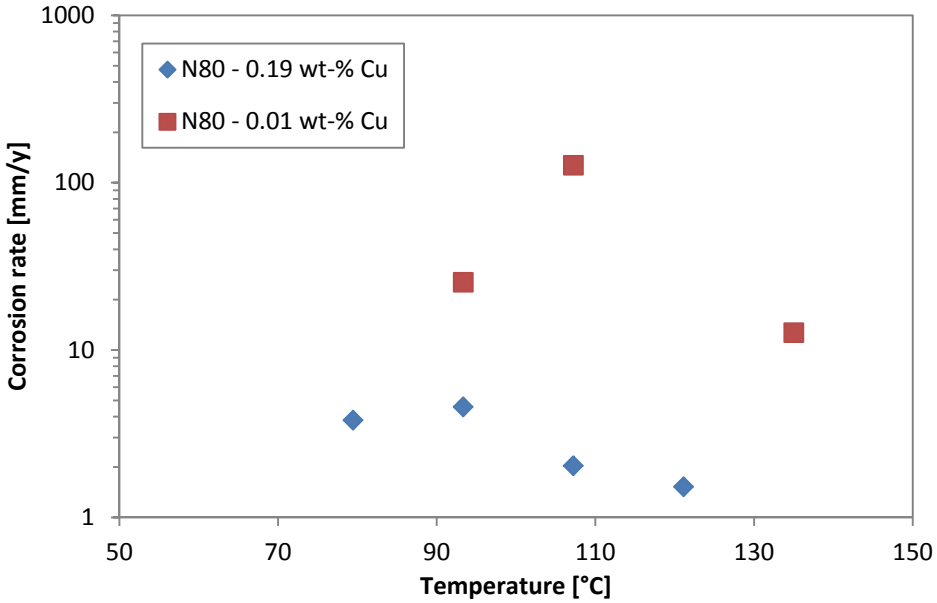

Figure 10 – Effect of copper on N80 steel grade. Exposure time 100 hours, 69 bar partial pressure CO_2 and 6 m/s flow velocity [8].

At high temperatures of 150°C or more, Fe_3O_4 is the stable scale, which will form a protective layer and decrease the corrosion rate. However it was found that upon the addition of copper, the temperature of Fe_3O_4 formation shifts to lower values of around 100°C. The rate at which Fe_3O_4 forms seems to be catalyzed by elements like platinum, nickel or copper, but not manganese. At temperatures below 90°C however, the copper seems to increase the corrosion rate due to accelerating the hydrolysis reaction of CO_2 thus increasing the corrosion rate [8].

Nickel

Two of the tested steels contained more nickel and the same amounts of chromium as the other tested steel grades, and their corrosion rate was higher than the others [31]. The author reports of other literature stating that a minimum level nickel reduced the corrosion rates of tubings.

Phosphor

Schmitt et al. [34] report of an unalloyed steel grade with an elevated level of phosphor to corrode faster than the other tested, unalloyed steel grades.

2.3 Influence of microstructure

Oil country tubular goods are manufactured according to API specification 5L. This specification only sets requirements such as yield strength, tensile strength and fracture toughness. Moreover, some chemical elements such as carbon, manganese, phosphorous and sulfur have concentration limits defined, to ensure weldability and formability. Hence, different levels of the mentioned elements as well as non-specified elements like chromium, copper, molybdenum or many more, together with different possible heat treatments like quenching, tempering, annealing or normalizing can lead to the full spectrum of possible microstructures. Since the microstructure has an impact on the corrosion processes and layer formation [38], more details on the influence of the corrosion rate are required.

As CO_2 corrosion is a very complex topic, it is not possible to simplify the matter by making the type of microstructure fully responsible for different corrosion effects. The viewer always has to see the bigger picture, with the influence of environmental parameters as described in 2.1.3 and the compositional influence as described in 2.2. In this chapter the results of other authors will be shown, and discussed. As there is no wrong or right, because of the mentioned complexity of this topic, different and controversial outcomes will be shown.

Crolet et al. [10] discussed the role of conductive corrosion products in the protectiveness of corrosion layers. In their paper they established, that the formed scales can either be extremely protective, have no effect, or even be corrosive. When corrosion happens, a galvanic couple between the insoluble $FeCO_3$ and the undissolved, cathodic Fe_3C can form. For the scale to be

protective, it has to be an empty layer of Fe_3C in which $FeCO_3$ can precipitate in direct contact with the surface. According to the author, this can only happen, if at the moment of the immersion, the medium was already saturated with iron ions so $FeCO_3$ can start to form immediately. For the other case, that no iron ions are apparent, a hollow Fe_3C layer will form and internal acidification will prevent a $FeCO_3$ formation in contact with the surface. Even though the outer part of this becomes obstructed, the resulting scale is not protective.

This example of how the formation of a scale takes place, explains why the distribution of carbon rich phase like pearlite, hence the microstructure is of such importance.

Clover et al. [39] studied the influence of microstructure on the corrosion rate of various carbon steels. An immersion test was performed at 50°C for two weeks with a CO_2 partial pressure of 3.4 bar. Corrosion rates were determined by mass loss measurements and penetration depth by an optical microscope. Their paper presented 34 steel qualities, which they assembled into four groups. Group 1, banded ferrite/pearlite microstructure, showed the highest mean penetration rates, whereas group 4, tempered martensite microstructure, showed the highest mean average corrosion rate. Group 2, very fine predominantly ferrite microstructure, and group 3, ferrite/coarser, and somewhat acicular pearlite/pearlite microstructure, showed similar corrosion rates, lower than for group 1 and 4 (Figure 11). The authors suggest that the poor performance of localized corrosion resistance of group 1 is because of the segregated distribution of the iron carbide phase cementite (Fe_3C).

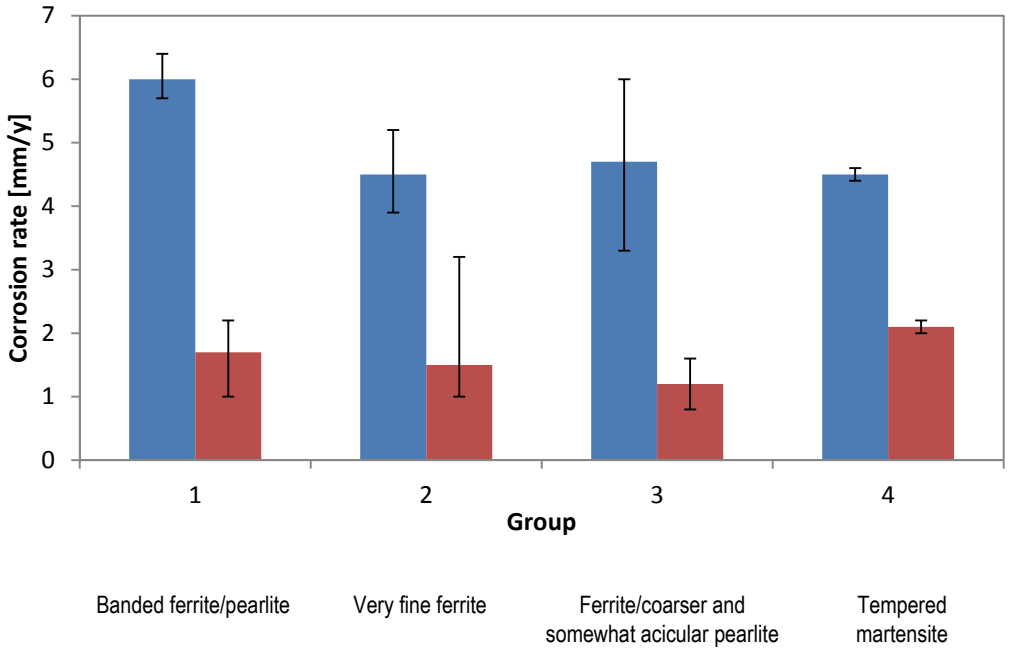

Figure 11 – Results of 34 tested steel qualities with various microstructures. Group 1: banded ferrite/pearlite; Group 2: very fine ferrite; Group 3: ferrite/coarser, and somewhat acicular pearlite; Group 4: tempered martensite. Blue bars represent mean penetration rate, red bars mean average corrosion rate. Black bars are min-max errors.

Palacios et al. [11] support the idea, that scale formed on normalized samples is more dense and thicker than on quenched and tempered samples. As ferrite corrodes away, the pearlite phase is left behind and cavities between the platelets form. Due to local flow stagnations and increased Fe^{2+} concentration, iron carbonate scales form easily and get anchored by the platelets. As there are no homogenously distributed cementite phases in tempered martensitic microstructures, neither the anchoring, nor the increased local Fe^{2+} concentration can occur. The more uniform the distribution of pearlite colonies is, the less is the corrosion rate [40]. Data shown by Chitwood et al. [41] also shows a superior behavior of normalized steels compared to quenched and tempered samples. Although no explanation was given, the authors state that grains of pearlite increase corrosion resistance, whereas decomposed pearlite, as received after tempering, has a detrimental effect. However, the authors close that the pronounced effect of microstructure on the corrosion resistance is rather rare, and only observable for special environmental conditions.

Other authors, like Mishra et al. [40] reported, that quenched and tempered structures corrode slower at low temperatures compared to normalized structures. This effect becomes predominant at long exposure times at lower temperatures, and decreases to almost no difference at 60°C or higher (Figure 12).

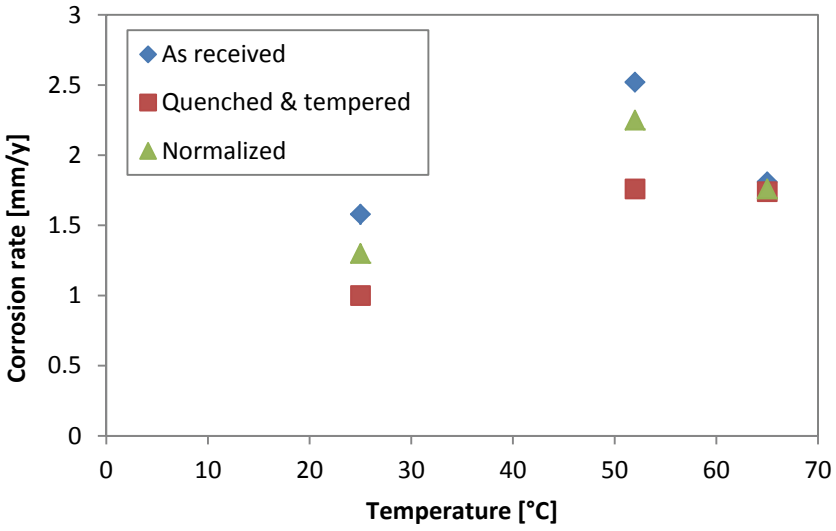

Figure 12 – Corrosion rate for various heat treatments for X52 steel as a function of temperature, at a partial pressure CO_2 of 0.86 bar, 800 hours exposure time and a pH of 5.2-5.7 [40].

This was shown again by Al-Hassan et al. [37] in Figure 13. The corrosion rates of the as-received and normalized samples was always higher than those of the quenched and tempered and annealed ones. The as-received, which is coarser than the normalized, and the normalized qualities have homogenously distributed pearlite phases. The annealed quality has segregated bands of cementite; the quenched and tempered quality shows a tempered martensitic microstructure. The authors explain the behavior of increased corrosion speed for as-received

and normalized qualities with the increased contact area of Fe_3C to the solution, as ferrite corrodes away, leading to larger cathodic sites. However as the annealed samples deviated from this behavior, the authors suggested that the surface area of contact between pearlite and ferrite was more important in determining the corrosion rate than the contact area between pearlite and solution. Assuming that the amount of pearlite phase is equal in the annealed and normalized microstructure, then the contact area between banded pearlite phases and ferrite is smaller than between globular pearlite sites and ferrite.

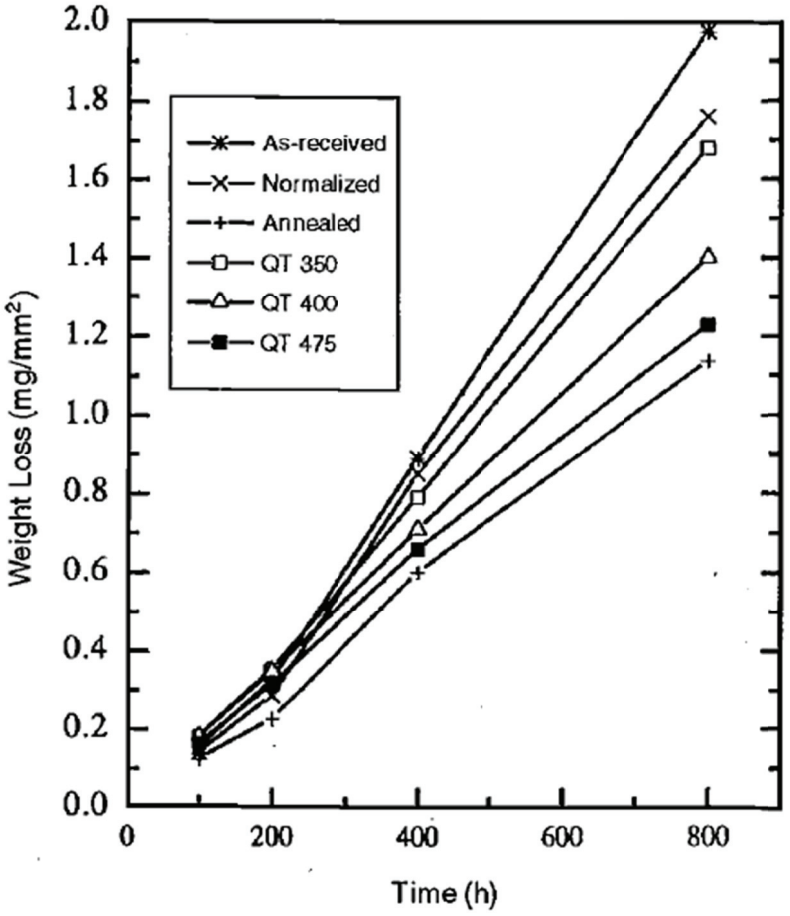

Figure 13 – Weight loss in CO_2 containing aqueous solutions at 1 bar for X-52 steel as a function of time at 58°C and a volume-to-surface area ratio of 4.4 ml/cm² [37].

The same authors [37] investigated the corrosion behavior of pure ferrite and pure, eutectoid pearlite. The eutectoid sample was reported to have corrosion rates 4-6 times higher than the pure ferrite, which had the lowest corrosion rates of all performed tests.

Even researchers from the same work group, achieve different results for the same experiment. Paolinelli et al. [42] performed the same experiment as Lopez et al. [43; 44] a few years earlier. Both used a carbon steel with the chemical composition 0.99 Mn – 0.38 C – 0.33 Si – 0.17 Cr – 0.09 Cu – 0.04 Ni – 0.02 Mo – <0.01 P – <0.01 S – Fe balance with an annealed (ferritic-pearlitic) and a quenched and tempered (tempered martensitic) microstructure. Both

experiments were conducted at 40°C in a stirred environment with a volume of 0.5l. The test solution was adjusted to a pH of 6 by the addition of $NaHCO_3$. Even though test parameters, chemical composition and microstructure were identical for both tests, different results were reported in their work respectively. Lopez et al. explained the higher corrosion rate of the annealed samples with the increase in cathodic area. When the ferrite of the sample is corroding, a laminar structure of non-oxidized $FeCO_3$ is not removed. In contrast, on the quenched and tempered samples, the globular cementite detaches, as the ferrite which encloses it, corrodes away. Therefore, the area of exposed cementite increases over time for the annealed samples as does the corrosion rate. Paolinelli et al. on the other hand explained the beneficial behavior of the ferritic-pearlitic structure of the annealed samples with its local increase in ferrous ions due to the left behind cementite lamellae. A precipitation could be favored compared to the tempered martensitic microstructure. Moreover can the lamellae help in anchoring the scale and therefore contribute to improved scale properties.

The effect of anchoring the $FeCO_3$ scale has also been attributed to the needle like quenched and tempered microstructure by Stegmann et al. [8]. The quenched and tempered L80 showed less corrosion rate than the AISI-1010 grade, which has large ferrite areas interspersed by pearlite grains. AISI-1010 grade showed higher perception to mesa-type corrosion than the L80.

In the work of Vega et al. [45] four different microstructures of an API 5L-X42 steel were investigated: banded, normalized, quenched and tempered, and annealed. Electrochemical impedance spectroscopy experiments were conducted at atmospheric pressure and room temperature in a CO_2 saturated solution at a pH of 3.8. The results show the highest polarization resistance and thus the lowest corrosion rate for the annealed samples, followed by quenched and tempered, normalized and at last the banded samples (Figure 14). XPS analysis revealed a stronger iron carbonate signal for the annealed and the quenched and tempered microstructures. This is in agreement with the EIS measurements, as the existence of $FeCO_3$ is related to the corrosion rates.

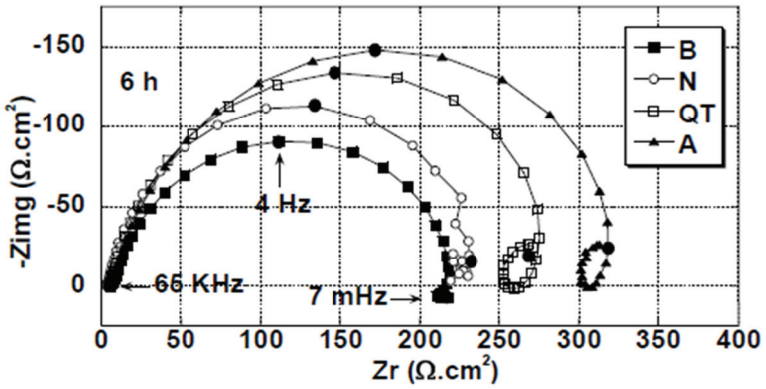

Figure 14 – Impedance diagrams obtained at the corrosion potential for different steel microstructures after 6 hours of immersion in CO_2 saturated, artificial, 3.5% NaCl brine. B: Banded; N: Normalized; QT: Quenched and tempered; A: Annealed.

No correlation between microstructure and corrosion rate was reported by Dugstad et al. [31]. The high corrosion rates found for tempered martensitic structures were explained with the low chromium content, as the bainitic martensitic ones, which contained more chromium, corroded slower. The corrosion rate of the ferritic pearlitic structure showed a similar behaviour, as it was high for low chromium content, and decreased as chromium content was increased.

From this brief literature review, everyone can see that there is no general consensus in the technical literature. The influence of the microstructure seems to be a part of the corrosive system, but not the driving factor, if there even is one. As mentioned before, every parameter has to be taken into account before judging the effect of a single one.

2.4 Influence of grain size and band-type formation

Not much effort has been put into the investigation of exclusively those two effects. In some literature, the authors note that there could be an influence. There seems to be no direct correlation between grain size of different phases and the corrosion rate, but generally the smaller the ferrite grain size, the lower the corrosion rate [40]. However Al-Hassan et al. [37] showed that for pure ferrite samples, a higher annealing temperature of 960°C compared to 920°C results in lower corrosion rates [37]. They attribute this phenomenon to less grain boundaries due to increased grain size. The grain size was thought to be cathodic in pure iron samples.

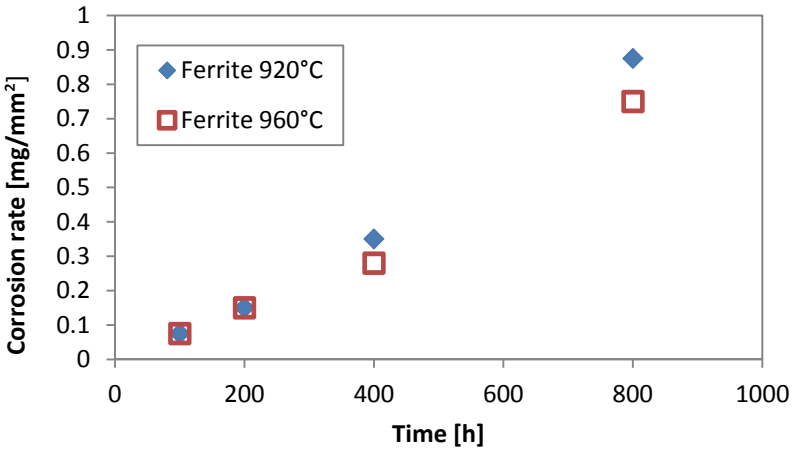

Figure 15 – Weight loss in CO_2 containing aqueous solutions at 1 bar for pure α–iron samples as a function of time at 51°C and a volume-to-surface area ratio of 4.4 ml/cm² [37].

Due to segregated cementite bands, localized corrosion was promoted in a ferrite/pearlite structure. However, no increased mean corrosion rates were reported [39]. Al-Hassan et al. [37] measured lower corrosion rates for annealed samples with segregated cementite bands. They attribute this behavior to the smaller contact area of pearlite to ferrite compared to normalized samples.

3 Experimental part

3.1 Test specimen

3.1.1 Sampling

Samples were taken from various tubing qualities with various heat treatments. The supplier delivered both ends with the upset, and a body part of each tubing quality. Henceforth, only the bodies were used. Heat treatment of J55 Q&T grades was performed at OMV Laboratories, the other grades were heat treated by supplier. In order to compare the results, the steel grades were sorted into L80 grades plus the 1%Cr normalized proprietary grade, the J55 grades and the C1020 grade.

The L80 grades differed in chromium content, but were subject to the same heat treatment. For this experiment, the 1% normalized proprietary grade was grouped together with the L80 grades, as it has comparable mechanical properties and chemical composition. The J55 grades, referred to as C-low and C-high, differ in their amount of carbon and other chemical elements, as well as microstructure. The C1020 grades represent the standard corrosion coupon of the laboratory. Old and new refer to different batches and the grades have minor chemical compositional differences (Table 2).

All samples were numbered with their sample number, plus a continuous number, so that each coupon had a unique number. C1020 samples did not have to be numbered, as the supplier already numbered them.

Table 2 – Sample details, heat treatment information and hardness in Vickers. As rolled: no heat treatment performed; N&T: normalized and tempered; Q&T: quenched and tempered; 2 x N: two times normalized. C1020 taken from two different batches, referring to as old and new.

Sample number	Grade	Heat treatment	Hardness [HV]
1	1%Cr normalized	N&T	226
6	L80	Q&T	236
3	L80 1%Cr	Q&T	225
26	L80 3%Cr	Q&T	253
15	J55 C-high	As rolled	191
24	J55 C-high	2 x N	180
31	J55 C-high	Q&T	204
12	J55 C-low	As rolled	213
18	J55 C-low	2 x N	194
32	J55 C-low	Q&T	204
--	C1020 old	As rolled	129
--	C1020 new	As rolled	130

3.1.2 Sample preparation

Two sets of corrosion coupons were manufactured and all samples had the same geometry as shown in Figure 16. Sample thickness was 3 mm. The first set was cut and milled out of the tubing material, the surface was smoothened and sand blasted with corundum. Prior to testing, the coupons were degreased by rinsing with acetone. The second set was also cut and milled out of the tubes and afterwards smoothened. Prior to the testing the surface layer was removed by polishing with wet, 320 grit silicon carbide paper and samples were rinsed with acetone to remove any traces of grease.

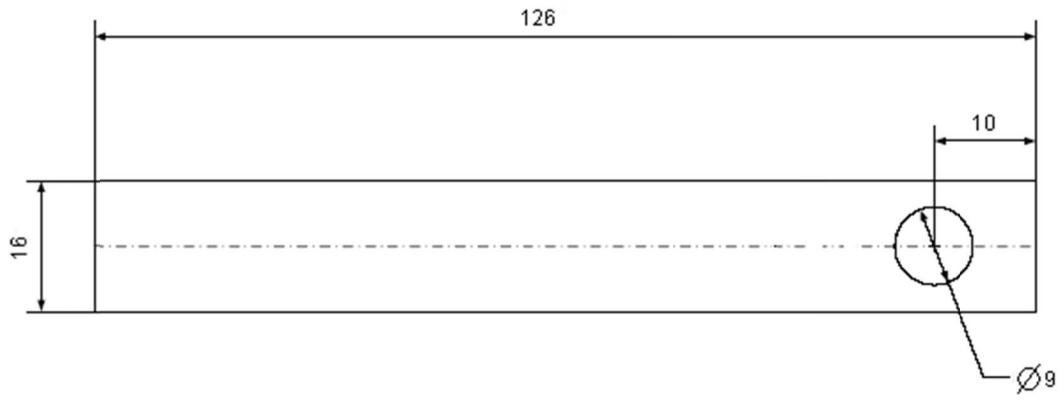

Figure 16 – Sample geometry in mm. Sample thickness was 3 mm.

3.1.3 Chemical composition

Chemical analysis was done with a MA3460 Metal Analyzer by Applied Research Laboratories. The analysis of all tested samples is shown in Table 3. It is worth noting that the heat treatment did not change the chemical composition, thus it is possible to compare the microstructure without effects of changed composition.

Standards were tested before and after analyzing the samples, to ensure exact measurements. All elements were within the limits of the API 5CT and OMV specification.

Table 3 – Chemical composition of examined samples; all values are weight%; elements with no value were out of the working range; the remaining composition is Fe.

Grade	Number	Heat Treatment	C %	S %	Mn %	Cr %	Mo %	Cu %
L80	6	Q&T	0.247	*	1.34	0.055	0.021	0.162
L80 1%Cr	3	Q&T	0.271	*	0.70	1.034	0.196	0.171
L80 3%Cr	26	Q&T	0.086	*	0.49	3.095	0.304	0.228
1%Cr norm.	1	N&T	0.37	*	0.91	1.043	0.119	0.162
J55 C-high	15	As rolled	0.38	0.00144	0.65	0.141	0.025	0.145
J55 C-high	24	2 x N	0.38	0.00169	0.66	0.142	0.026	0.146
J55 C-high	31	Q&T	0.38	0.00175	0.66	0.140	0.025	0.146
J55 C-low	12	As rolled	0.28	0.00604	1.40	0.077	0.026	0.227
J55 C-low	18	2 x N	0.29	0.00284	1.39	0.063	0.026	0.212
J55 C-low	32	Q&T	0.29	0.00273	1.35	0.079	0.014	0.200
C1020 new	--	As rolled	0.20	0.00192	0.52	0.097	0.008	0.102
C1020 old	--	As rolled	0.18	0.01131	0.46	0.032	0.004	0.049

Grade	Si %	P %	Ni %	V %	W %	Ti %	Al %	B %	Nb %
L80	0.286	0.0119	0.088	0.0048	0.0081	0.0370	0.031	0.0020	0.0040
L80 1%Cr	0.257	0.0117	0.118	0.0038	0.0085	0.0032	0.023	0.0002	0.0034
L80 3%Cr	0.289	0.0139	0.034	0.1358	0.0100	0.015	0.034	0.0001	0.0050
1%Cr norm.	0.43158	0.014	0.109	0.0044	0.0091	0.006	0.030	0.0002	0.0037
J55 C-high	0.20048	0.016	0.100	0.0018	0.0073	0.003	0.026	0.0001	0.0026
J55 C-high	0.20183	0.017	0.100	0.0018	0.0075	0.003	0.026	0.0001	0.0026
J55 C-high	0.20382	0.017	0.101	0.0018	0.0078	0.003	0.027	0.0001	0.0028
J55 C-low	0.21496	0.013	0.110	0.0036	0.0092	0.032	0.027	0.0003	0.0035
J55 C-low	0.18764	0.014	0.113	0.0040	0.0076	0.031	0.024	0.0002	0.0035
J55 C-low	0.18974	0.018	0.078	0.0040	0.0084	0.032	0.026	0.0002	0.0033
C1020 new	0.09117	0.012	0.032	0.0018	0.0056	0.002	0.023	0.0001	0.0028
C1020 old	0.01099	0.009	0.032	0.0016	0.0051	0.001	0.051	0.0002	0.0029

3.1.4 Mechanical properties

Mechanical properties were taken from the data sheet of the manufacturer and were within the applicable specs.

The hardness of the samples was tested according to ISO 6507. To determine the hardness of the material, the measurement was performed using a Vickers diamond with a load of 10 kiloponds (Table 2).

3.1.5 Microstructure

Each sample was prepared by cutting two perpendicular parts (axial-radial and axial-tangential) and embedding in Buehler EpoMet G Molding Compound with a Struers LaboPress-3. Each sample was wet ground by MD Piano 80 and MD Piano 120 plate on a RotoPol-31 with a RotoForce-4 add-on. Subsequently the samples were diamond polished in three steps on the same machine used for grinding: (1) MD Allegro with 9 µm diamond spray, (2) MD DAC with 3 µm diamond spray, (3) MD NAP with 1 µm diamond spray. “Lubricant Blue” by Struers was used in all polishing steps. Grinding and polishing equipment by Struers was used. After each step the samples were rinsed with ethanol and dried to prevent traces of corrosion. The polished samples were etched with 3% Nital (nitric acid in ethanol). Microstructural examination was performed using a Zeiss Axiovert 200 MAT with a mounted AxioCam HRc camera by Zeiss. Each specimen was characterized in terms of their microstructure and band-type formation.

3.1.6 Heat Treatment

The heat treatment of samples 31 and 32 was performed using a Linn High Therm Muffle Furnace LM512-M. A semi-shell of the tubing was austenized at a temperature of 880°C for 30 minutes and subsequently water quenched. To minimize the Leidenfrost effect the semi-shells were moved around in the water. Afterwards the samples were tempered for 120 minutes at 700°C followed directly by air cooling. The achieved microstructure was tempered-bainitic and had the same hardness and chemical composition as the primary material.

To achieve an oxygen free environment for the coarse grain heat treatment, two measures were taken:

1. the muffle furnace was constantly flushed with N_2 at rate of 50 liters/hour;
2. the samples were sealed in stainless steel foil, to further reduce the amount of oxygen it is in contact with.

All attempts to produce a coarse grain were in vain. No parameters could be found, where a grain size of at least 3 could be measured. Furthermore the high temperatures and long exposure times in the furnace led to carbon depleted samples and thick oxide scales (Figure 17).

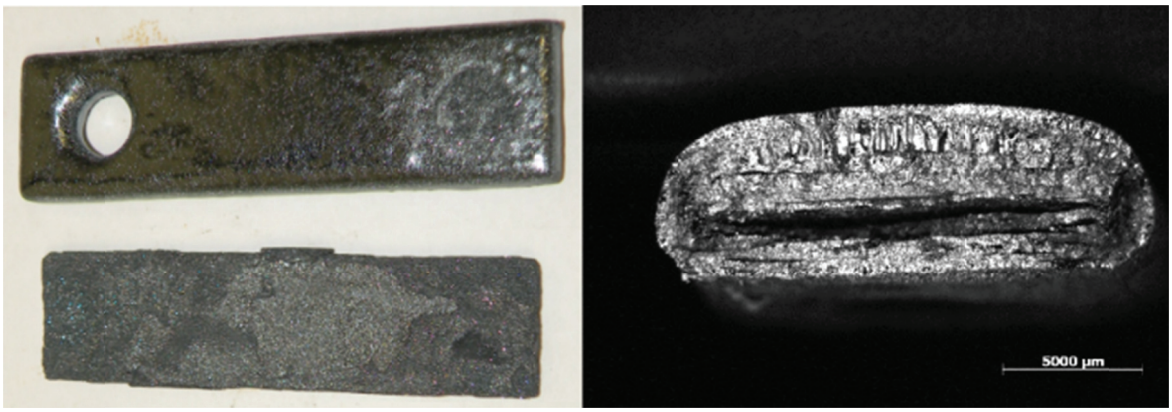

Figure 17 – Coarse grain samples. Top one without stainless steel foil, bottom one with. Both were carbon depleted and had oxide layers. Coarse grain samples were not used in the actual test.

3.2 Corrosion tests

3.2.1 Autoclave tests

Corrosion testing was performed by means of the autoclave wheel test method, where a rotating axis is installed in a heating cabinet (Figure 18). Autoclaves (Figure 19) are mounted onto this wheel with clamps, ensuring a continuous rotation and therefore a repeated wetting of the samples by the test fluid.

Figure 18 – Autoclaves installed on the wheel in the heating cabinet.

Table 4 – Composition of artificial brine in autoclave tests.

	Concentration [g/l]
NaCl	52.31
$CaCl_2 * 2H_2O$	2.77

Figure 19 – Samples in Teflon arrangement and autoclave.

The weight of the corrosion samples was measured before the test using an analytical balance and the dimension of each specimen was noted to evaluate the surface area of each sample. The coupons were activated prior to the test by using a brush and a fine scouring powder to remove inhibiting substances.

The autoclaves were evacuated to ensure an oxygen free environment and filled with the corrosion medium (Table 4) and were pressurized to an initial pressure of 26 bar CO_2 at room temperature. After being installed in the heating cabinet, they were kept there for 120 hours and a constant temperature of 80°C. The pressure at 80°C was calculated to be 33 bar. The difference in the calculated pressure between the ideal gas equation and a model which takes the compressibility factor z into account [46] was determined to be less than 3% hence the ideal gas equation was used.

To increase the precision of the testing method, a more reproducible and exact flow of work, compared to regular testing for standard tests, was specified and performed. Prior to all testing, every coupon was degreased with acetone and ground with #320 silicon grinding paper: First the edges, then the plane, followed by immediate drying in acetone afterwards. After that, the coupons were measured and weighed and assembled with the Teflon mounting into the autoclave. Then, the autoclave was evacuated for at least one minute, to a pressure less than 15 mbar. This process was repeated for all coupons.

To test the leak-tightness of the valves, every autoclave was filled with 50 bar N_2. A valve was checked for leaking in two ways:

1. A leak detection spray by Alltec was sprayed on the valves. In the case of a leak, bubbles formed on the leaking spot.
2. In a separate test, all autoclaves were filled with 50 bar Helium and the initial pressure was measured. After a period of a few days, the pressure was measured again. Autoclaves which lost more than 10% of their initial pressure were assumed to be leaking.

Any leaking valve was replaced by a tight one. The coupons of the leaking autoclave were handled as delivered, and had to be prepared anew.

Prior to being filled with the testing medium (Table 4), the autoclaves had to be evacuated again to the specified pressure, to empty the autoclaves of the N_2 atmosphere. After all autoclaves were filled with the testing fluid, 26 bar of CO_2 gas was pressed into the autoclaves. In the next step, all autoclaves were mounted in the heating cabinet for the next five days at a temperature of 80°C. In a separate test it was measured, that about 25% of the initial gas dissolve in the water, leaving a pressure of about 18 bar at room temperature and 26 bar at 80°C in the autoclaves. This measurement goes hand in hand with an iterative calculation performed using data provided by Duan et al. [17].

Fitting the data of Duan et al., the solubility of CO_2 in water can be calculated for known pressures. As the system is closed after pressurizing, the volume - and therefore the mole of gaseous CO_2, as well as the temperature - as the autoclave is in the heating cabinet, are constant. Thus the only changing variable in the calculation is the pressure, which changes due to the solution of CO_2 molecules in the brine. As the gaseous molecules solve, and the pressure decreases, the solubility of CO_2 in H_2O decreases as well, which results in a higher pressure than initially calculated. Therefore the equilibrium state had to be calculated by iterative means.

At the end of the testing time, the heating cabinet was opened and the heater was switched off. As soon as all autoclaves were cooled down, the demounting started. First, the pressure of each autoclave was tested using a Digibar®II PE300 by HBM. Then the valves of all autoclaves were opened before disassembling.

After disassembling, the materials were cleaned and pickled in a few steps, to free them from corrosion products and the carbonate scale:

1. coupons were dried using acetone;
2. coupons were pickled in an acid mixture (49.75% deionized H_2O, 49.75% concentrated HCl, 0.5% Cronox 242ES) at room temperature for 3 minutes;
3. subsequently, the coupons were brushed with fine scouring powder (ATA by Henkell) and dried;
4. coupons were pickled at 50°C in the same acid mixture;

5. after drying, the coupons were put in an desiccator overnight, to minimize the effect of the time between pickling and weighing;
6. finally the coupons were measured and weighed to quantify the mass loss.

To verify the repeatability of this testing method, an examination of the corrosion rate of C1020 coupons with the same parameters in the same environment was conducted. This showed two things: first, the results of the tests are normally distributed, and second, the corrosion rate is consistent within each autoclave, even for mathematically eliminated outliers. Although the statistical spread reaches from about 0.5 mm/y to approximately 1.5 mm/y in each test, the mean value over all the tested samples was about 1.0 mm/y in both tests.

3.2.2 Electrochemical tests

A schematic picture of the electrochemical cell used is shown in Figure 20.

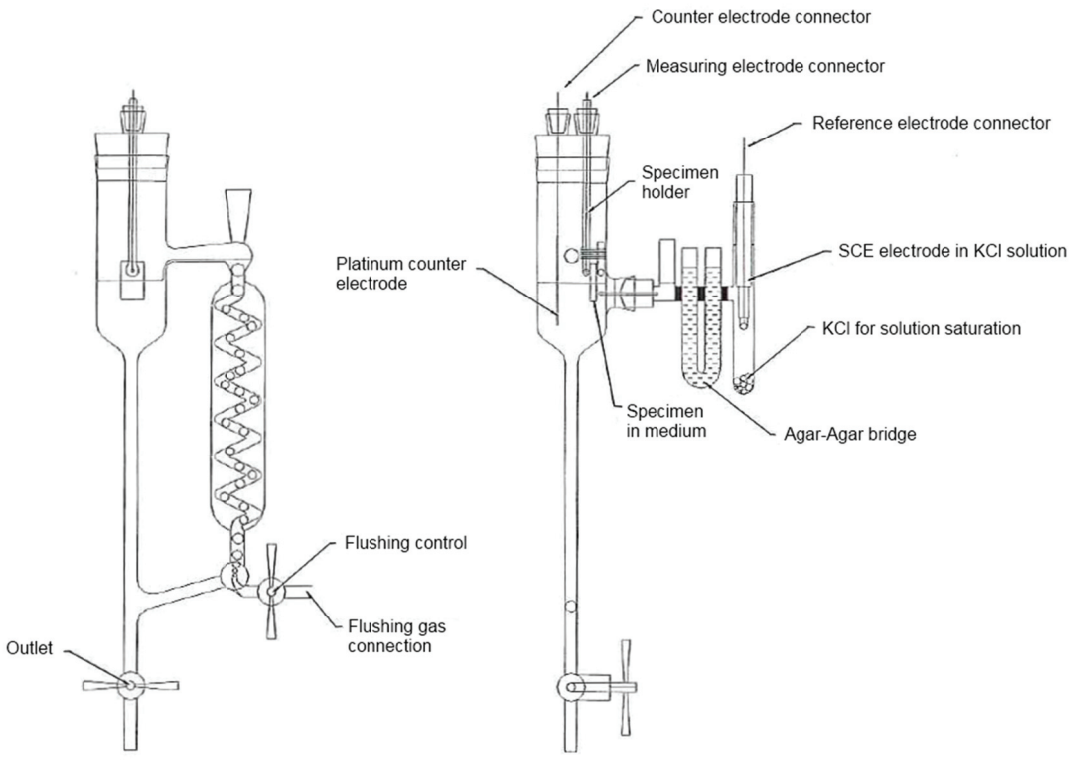

Figure 20 – Electrochemical cell used for linear polarization measurements.

The cell consists of three parts

- Testing cell
- Potentiostat to build up the polarization potential and to measure the corresponding current
- PC to control the potentiostat and to process the data

As testing medium, the artificial brine as described in Table 4 was used. It was bubbled with CO_2 at 1 bar for 30 minutes prior to testing. Testing temperature was set to 80°C and controlled with a thermostat. The specimen holder consisted of two glass tubes which were held together by a plastic band to form a clamp. In one of the glass tubes a platinum wire was inserted which ended in a platinum button, to establish a connection to the sample.

As counter-electrode a platinum plate (10 x 60 x 1 mm) was used. It was cleaned with concentrated HCl and heated until recrystallization. Both sample and counter-electrode were in the testing cell. The reference-electrode was connected to the testing cell via a salt bridge composed of Agar-Agar-Gel. A standard calomel electrode dipped in saturated KCl was used as the reference-electrode.

The following steps were performed during the measurement of the current density-potential-curve:

1. Testing medium was heated to the designated temperature and bubbled for 30 minutes with CO_2.
2. Open circuit potential (OCP) was measured for 30 minutes.
3. Begin of the polarization 100 mV below OCP; potential scan rate was 200 mV/h; reversal condition was set to 2 mA/cm^2.
4. When the measurement was finished, the samples were cleaned with acetone and dried.

3.3 Test evaluation

3.3.1 Autoclave test evaluation

The following formula was used to evaluate the corrosion rate from autoclave testing (11):

$$CR = \frac{365 * \Delta m}{\rho_{(Fe)} * d * A} \qquad (11)$$

where "Δm" is the weight loss [g], "$\rho_{(Fe)}$" represents the density of iron [g/mm^3], "d" stands for the days the experiment lasted [days] and "A" is the surface area of the samples [mm^2]. The factor 365 is used to convert the corrosion rate from [mm/d] to [mm/y].

The corrosion rates were plotted against the materials and the chemical composition. Furthermore the correlation between the microstructure and the corrosion rate was evaluated. All values were checked for outliers with Dixon's Q-Test with a confidence of 95% [47].

3.3.2 Electrochemical test evaluation

For the evaluation of the current density-potential-curves Tafel slopes were determined. Figure 21 shows the use of Tafel slopes, to obtain the intercept point of the slopes of the tangents to the anodic and the cathodic curve and the OCP [48]. The intercept point is called the corrosion-current-density with the units [mA/cm^2] which can be used to calculate the corrosion rate [mm/y]. To convert one into the other, the factor shown in equation (12), which is only valid for iron, due to its electron valence and density, is used [49]:

$$1\,mA/cm^2 = 11.6\,mm/y \qquad (12)$$

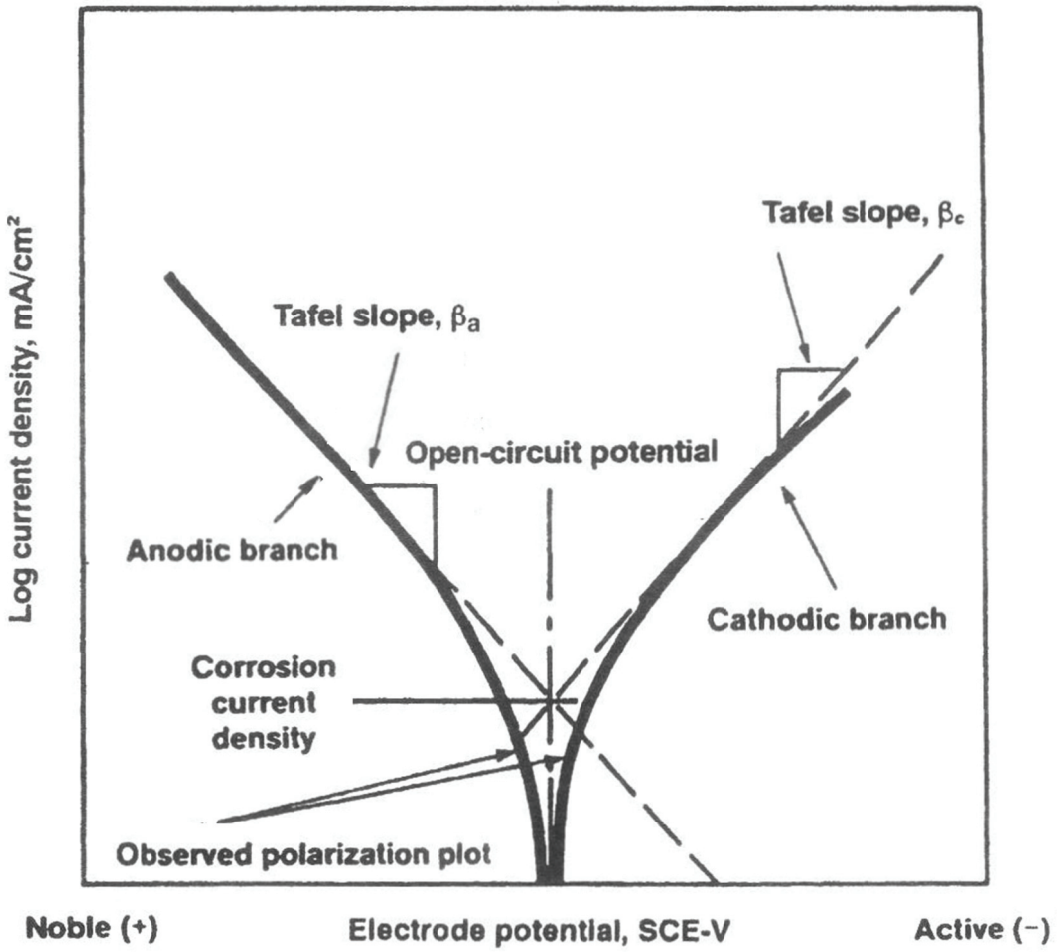

Figure 21 – Anodic and cathodic polarization curves for an active metal in deaerated acid [48].

Figure 21 shows the ideal case of a current density-potential-curve where the Tafel slopes can be used to obtain exact and unique values, whereas Figure 22 shows a measured curve. The great number of possible tangents shows, that for the obtained corrosion rates a large scatter had to be considered.

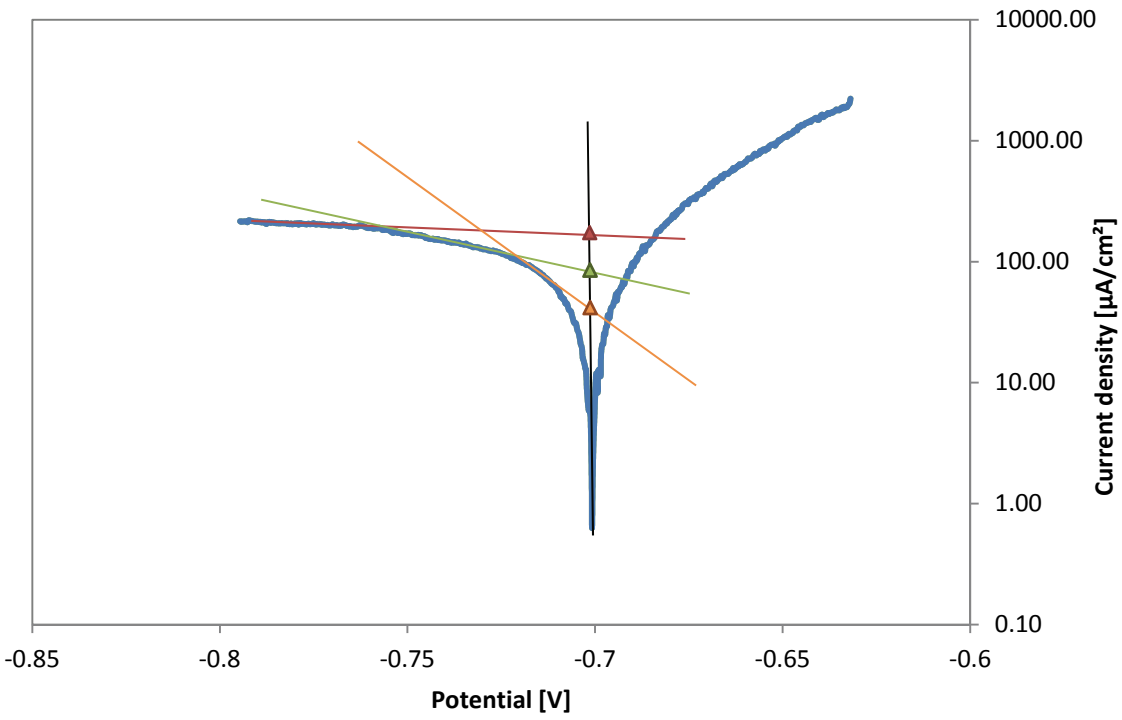

Figure 22 – Current density as a function of potential. Tangents on anodic branch show possible intercept points (triangles) with open-circuit potential to find corrosion current density.

The results of the electrochemical tests will be discussed in chapter 5.9 in detail.

3.4 Statistical evaluation

Two statistical tools were used on the measured data: the Kolmogorov test to verify if a set of data is normally distributed, and the Student's t-test to confirm if the null hypothesis applies.

This chapter explains the standard principles of both tests. For more detailed information and formulas, refer to the cited literature.

3.4.1 Kolmogorov test

The Kolmogorov test [50] proves whether the measured data are normally distributed; hence whether the Student's t-test as described in 3.4.2 can be applied. This test was used because only small amounts of samples were tested. The following steps were performed on all acquired data.

1. The characteristic values were sorted in ascending order.
2. Characteristic values were z-transformed to evaluate the area below the Gaussian curve.

3. The area ranges, which should be equal for normally distributed values, were evaluated and summarized to show the ideal area below the Gaussian curve.
4. The difference between the calculated area and the ideal area is the statistical value, which can be compared to a tabulated value.
5. If the statistical value is below the tabulated value, normal distribution is present.

All data were proven to be of normal distribution.

3.4.2 Student's t-test

The Student's t-test [51] is one of the most commonly used techniques for testing the null hypothesis (13) between two independent populations. If the null hypothesis applies, no statistical difference between their mean values can be distinguished.

$$\mu_1 = \mu_2 \tag{13}$$

where μ_1 and μ_2 are the mean values of two populations.
The null hypothesis cannot be rejected if the calculated t-value is smaller than the tabulated value. If the t-value is greater than the tabulated value, the alternate hypothesis (14) applies. The higher the value of t, the greater the confidence that there is a difference.

$$\mu_1 \neq \mu_2 \tag{14}$$

The following points were executed to get the t-values for all data. It is important to mention that each population has to be tested against every other. It has proven to be useful to write the calculations and results in the form of the right, upper half of a matrix, as shown in Figure 23.

1. The mean value of the characteristic value, its standard deviation and the degrees of freedom were calculated for each population.
2. The values for A and B were calculated.
3. t was calculated and compared to its tabulated value.

The formulas needed for this test are as listed below (15):

$$t = \left|\bar{x}_1 - \bar{x}_2\right| \div \sqrt{A * B} \tag{15a}$$

$$A = (n_1 + n_2) \div n_1 * n_2 \tag{15b}$$

$$B = [(n_1 - 1) * s_1^2 + (n_2 - 1) * s_2^2] \div (n_1 + n_2 - 2) \tag{15c}$$

where t is the statistical t-value, $\bar{x}_1$ and $\bar{x}_2$ are the mean values of the populations, n_1 and n_2 are the quantity of values and s_1 and s_2 are the standard deviations of the populations.

A-D	Population A versus Population B	Population A versus Population C	Population A versus Population D
B-D		Population B versus Population C	Population B versus Population D
C-D			Population C versus Population D

Figure 23 – Schematic figure of t-test results. Red color means that populations can be distinguished, black means the null hypothesis could not be rejected.

4 Experimental results

4.1 Results on test parameters

4.1.1 Influence of temperature

As described in 2.1.3 the highest corrosion rate should be, according to the literature, at around 80°C. To verify this for the used samples and testing method, a test was conducted.

A set of autoclaves was tested using the same medium and parameters as in 3.2, but over a temperature range from 40°C to 120°C. Figure 24 shows that the highest corrosion rates were achieved between 60 and 100°C with declining values on both sides of the peak. A t-Test was performed on the measured data, with the result of 40°C and 120°C being independent populations and the results between 60°C and 100°C not being distinguishable.

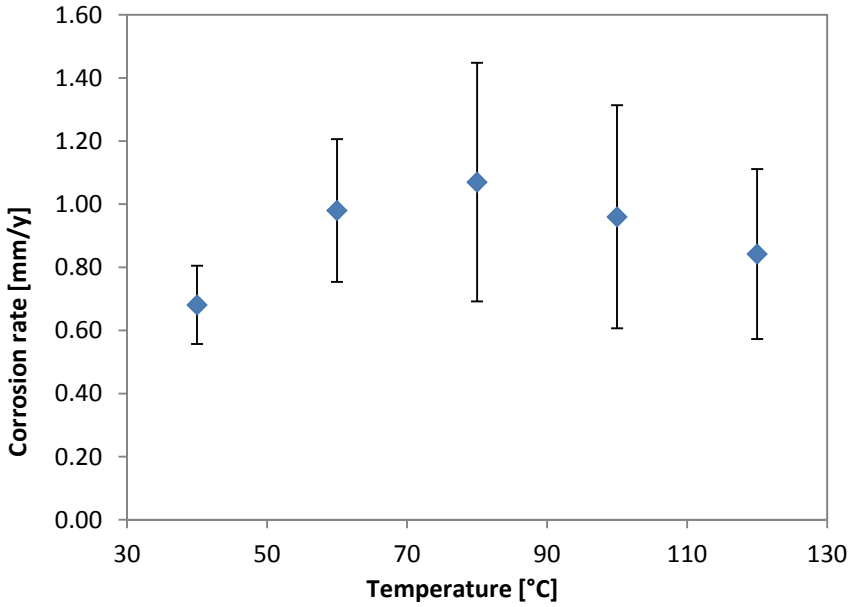

Figure 24 – Corrosion rate as a function of temperature at 26bar CO_2 filling pressure, 5% NaCl solution, 80 ml artificial brine and 5 days of exposure. Tested material was C1020. Bars represent standard error.

4.1.2 Influence of CO_2 partial pressure

A test was conducted to determine the effect of CO_2 partial pressure on corrosion rate. The tested material, medium, and temperature were selected as usual, and testing pressures were 1, 5, 13, 26 and 52 bar.

Figure 25 shows the results of the measurement. As discussed in chapter 2.1.3, the influence of the higher partial pressure and thus the lower pH becomes negligible. A t-test confirmed that apart from the 1 bar, the other pressures cannot be distinguished.

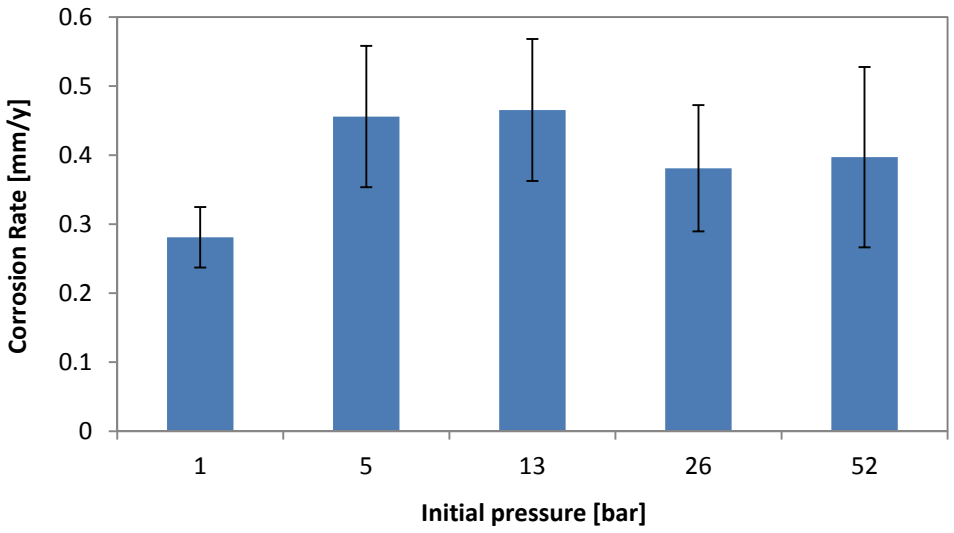

Figure 25 – Corrosion rate as a function of initial filling pressure CO2 at 80°C, 5% NaCl, 80 ml artificial brine and 5 days exposure. Tested material was C1020. Bars represent standard error.

To assure that enough gas is present for the reaction to not stop before the end of the testing time, and thus to keep the pH relatively constant, a pressure of 26 bar was selected for further tests.

4.1.3 Influence of the amount of used medium

An amount of 80 ml medium was used in all but the last tests. Throughout all those tests, a corrosion attack at the lower halves (Figure 26) of the coupons could sometimes be seen. The reason for this “half-side-corrosion” phenomenon can be found in the fact that this part of the coupons was continuously wetted. The upper part was out of the medium whenever the autoclave wheel turned around. This corrosion attack had several consequences:

- Different scale formation: The outer edges of the coupons which did not show this half-side-corrosion had a dense, black scale, which could not be removed by hand. The scale which formed on the lower parts however was easily removable, just by rinsing water over it.
- Different corrosion attacks: All coupons which showed the half-side-corrosion, had a higher corrosion rate than those which did not show this effect. This could be seen with mass loss measurements as well as by the decreased thickness and width and a very rough surface.

In order to avoid this phenomenon, for the finally valid experiments a volume of 50 ml was used. This helped to stop the unusual corrosion attack by ensuring that no part of the coupons was

exposed to permanent wetting. This led to dense and uniform corrosion scales on all of the tested coupons.

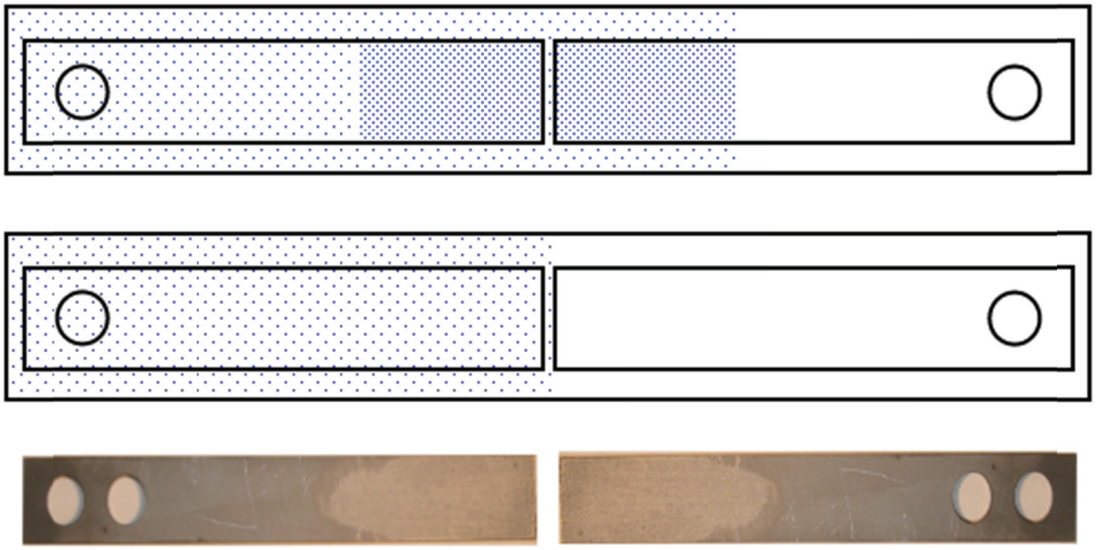

Figure 26 – Schematic of half-side corrosion and actual sample from experiment. Sparse blue dots show medium, 80ml for upper picture, 50ml for middle picture. Dense blue dots show the areas of increased corrosion attacks. Increased corrosion attack can be seen for the real coupon in the lower third.

The downside of using 50 ml instead of 80 ml is that the ratio of solution to coupon surface area decreases from approximately 1 ml/cm^2 to 0.6 ml/cm^2. As most authors in literature use a ratio of at least 20 ml/cm^2 (Table 1), the effect of such a low value and a further decrease should be investigated seriously, as corrosive reagents could become the limiting factor in the system. If the ratio is smaller, the corrosiveness could change through depletion of the corrodant or accumulation of corrosion particles.

4.1.4 Influence of exposure time

To study the influence of exposure time on the corrosion rate, 60 coupons were exposed to the same medium and environment, for different times. The result (Figure 27) shows how the corrosion rate decreases with increasing time.

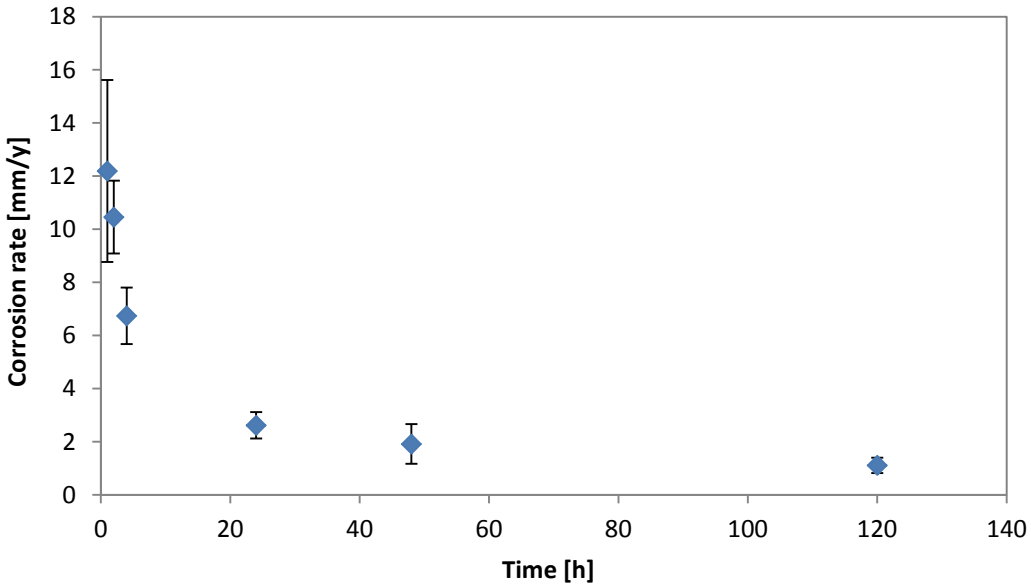

Figure 27 – Corrosion rate as a function of time at 80°C, 26 bar CO_2 filling pressure, 5% NaCl and 80 ml artificial brine. Tested material was C1020. Bars represent standard error.

This is an expected effect for several reasons. The most apparent one would be that the environment gets milder as the corrosion process consumes the corrosive agents. Another reason is that the coupons react with the CO_2 as described in 2.1.2., which can lead to the formation of a dense, protective layer [6; 9; 10; 11; 16; 52; 53; 54; 55]. A third reason is that at the very beginning of the experiment, the solution is free of $FeCO_3$ and it takes time until the medium is saturated so the carbonate can precipitate only after a certain exposure time.

To measure the correct corrosion rate of the material, and not starting effects, an exposure time of five days was defined. Longer times would have had no beneficial effects, and perhaps even worsened the resolution of the test. As shown inTable 5, the CO_2 was mostly used up for some autoclaves, and the corrosion would have stopped.

Mora-Mendoza et al. [56] showed some contrary results. When testing mild steel in CO_2 environments at different pH values, they reported an increase in the corrosion rate over time at higher pH values. They stated that due to the corrosion of ferrite, the surface area of cementite becomes larger over time, and therefore the cathodic area increases. A reason for not measuring these effects in our tests could be that a dense $FeCO_3$ scale was formed, which was not reported in the work of Mora-Mendoza for higher pH values.

It was also shown for low temperatures of 25°C by Al-Hassan et al. [37] that no decrease in the corrosion rate over time was measured. However upon increasing the temperature to 52°C and higher values, a decrease in the corrosion rate after about 400 hours was measured.

4.1.5 Final pressure after autoclave testing

When measuring the autoclave pressure after the testing time, a large range of values was measured. For the same parameters and environments, pressures between 12 and 19 bar were measured (Table 5). Two theories were developed to explain this phenomenon.

The first theory assumed that the autoclaves, or rather the valves, were not completely leak proof. So it was possible that a few autoclaves lost more gas than others. Some were not tight at all and lost the full pressure. To verify this theory, all autoclaves were filled with 50 bar Helium. After 5 days, the final pressure of all autoclaves was measured, and apart from leaking valves, which lost the total pressure, all were tight. This test was repeated with the same result, therefore theory one was shown to be wrong.

Theory two assumed that due to corrosion processes, the pressure rises. At the beginning of the experiment, the medium is free of CO_2 and the gas phase is full of it. CO_2, however, dissolves itself up to a certain concentration (exact value dependent of temperature and pressure) in the medium, where it reacts to H_2 following equations (3) and (4). Upon reacting, the saturation of CO_2 in the medium decreases, thus more CO_2 from the gas volume can dissolve itself. The evolving H_2 on the other hand, does not dissolve in the medium, and increases the pressure in the gas volume. This effect can be seen from Table 5, where the gas composition of a high and a low pressure autoclave was identified by gas chromatography.

Table 5 – Gas composition of high and low pressure autoclaves measured directly after immersion test. Parameters were 80°C, 26 bar CO_2 filling pressure, 5% NaCl and 5 days of exposure.

	High pressure	Low pressure
Components	[Vol%]	[Vol%]
Oxygen	0.03	0.02
Carbondioxide	15.44	59.85
Hydrogen	82.59	39.21
Rest	1.94	0.92

Another effect that can be correlated to different final pressures is the mass loss and the corrosion rate. However, when plotting the corrosion rates over the final pressures, the graph shows no trend. This is because the different steel grades used in this test show different corrosion rates. For the amount of gas that builds up in the autoclave, it is important how much iron reacts with the carbonic acid. Therefore, the mass loss of both coupons was summed up, before plotting over the final pressure. A clear trend can be seen in Figure 28, hence, theory two explains reasonably well the different final pressures.

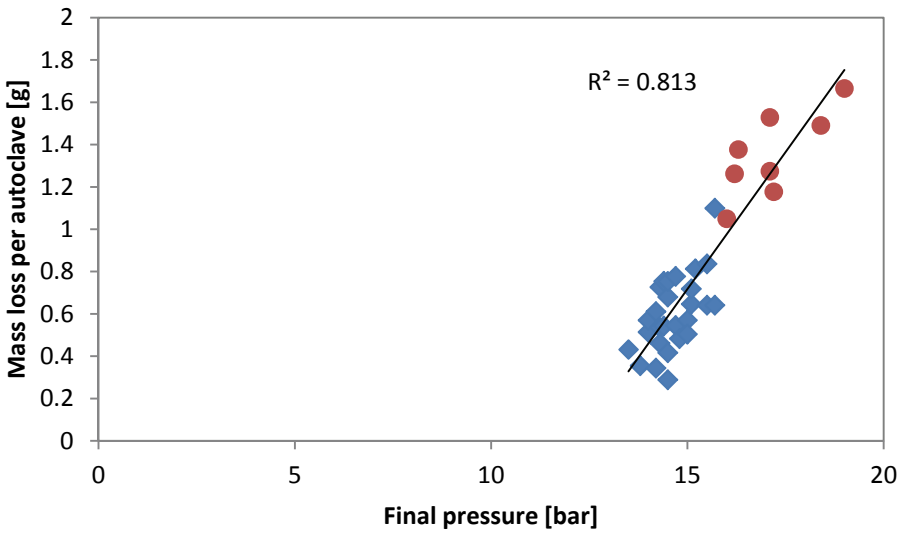

Figure 28 – Mass loss per autoclave as a function of final pressure measured after immersion test. Parameters were 80°C, 26 bar CO_2 initial pressure, 5% NaCl, 50 ml artificial brine and 5 days of exposure. Mass loss was taken from both coupons. Autoclaves containing C-Steels or 1% Cr steels are represented by blue squares, autoclaves containing 3% Cr steels are represented by red dots.

4.2 Results on different tubing materials

Figure 29 shows the results which will be discussed in the further sections. The main effect which was observed is a decreased variance of the values after using same surface condition, reduced amount of liquid and 5 days of testing to reach a quasi-steady state. Not a single outlier was measured in the course of this test, and the corrosion characteristics were the same for all coupons. Therefore, these results will be taken as the main outcome of this work and discussed in the following sections.

The influence of chemical composition will be discussed for both grades, separately and together, whereas microstructure, grain size and band-type formation will only be discussed for J55 grade, as the differences between the L80 samples are too small. Apart from these tubing samples, the differences between the C1020 standard coupon samples of the old and the new batch will be discussed.

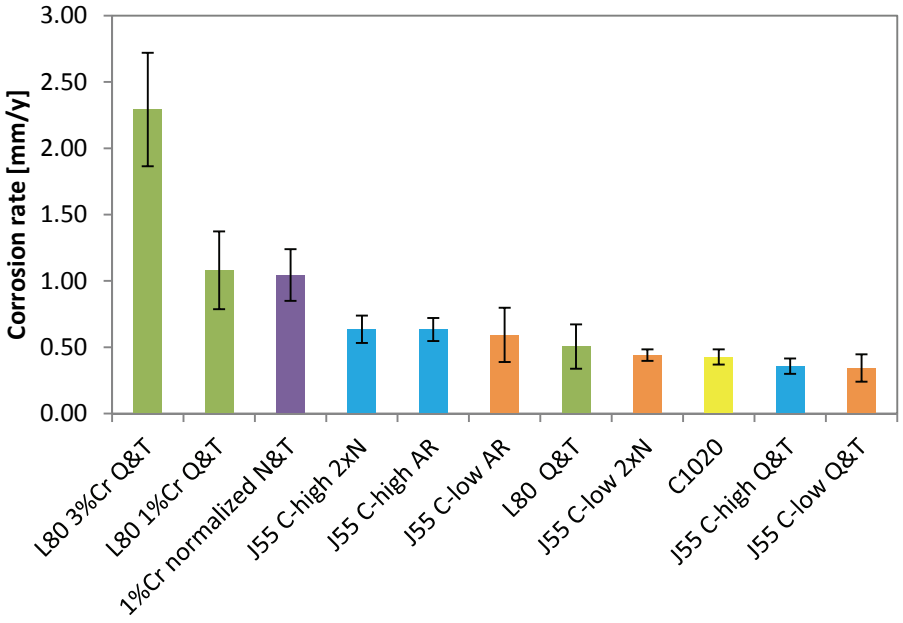

Figure 29 – Corrosion rate of the tested materials. Parameters were 80°C, 26 bar CO_2 initial filling pressure, 5% NaCl and 5 days of exposure. Bars represent standard error.

4.2.1 Analysis of chemical composition

Figure 30 shows the corrosion rate of the chromium free, J55 grades. The chemical composition of the different heat treatments is consistent within the C-high and C-low group of the J55 samples and is shown in Table 3.

For every available sample, the mean corrosion rate of the C-high samples was higher than the corrosion rate of the C-low samples. However, as the scatter bands of C-low AR as well as C-low Q&T are rather large, no significant difference, using student's t-test, could be calculated. For the twice normalized samples, the C-low shows significantly lower corrosion than the C-high sample.

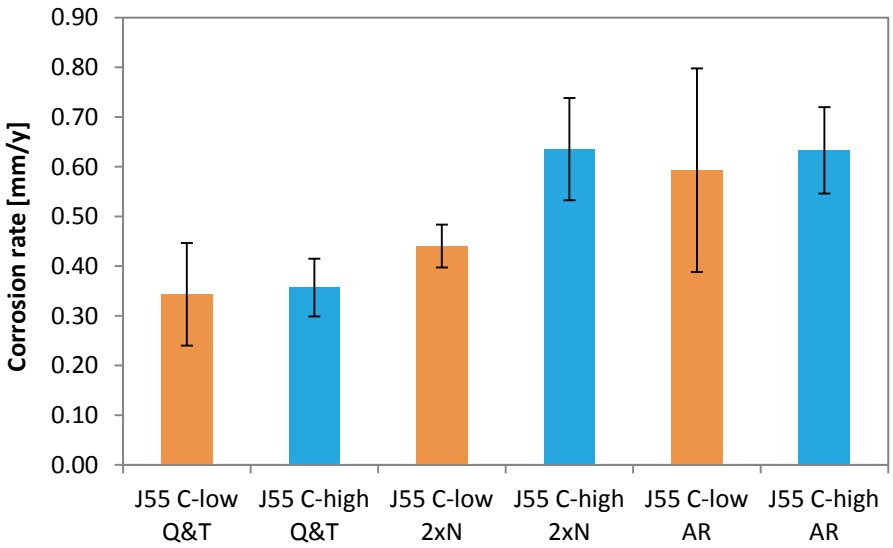

Figure 30 – Corrosion rate of J55 steel grades. Parameters were 80°C, 26 bar CO_2 initial filling pressure, 5% NaCl and 5 days of exposure. Bars represent standard error.

The carbon content has a constant value of 0.38 wt-% for the J55 C-high group, and 0.29 wt-% for the J55 C-low group. The manganese content is 0.65 wt-% for C-high and 1.40 wt-% for C-low. These are just two examples of all the chemical elements which were to be found in the samples and can similarly be done for all the others. However no trend could be seen for any element when plotting the corrosion rate over the chemical composition (Figure 31).

A discussion on the influence of microstructure on the corrosion rate can be found in chapter 4.2.2, respectively Figure 37.

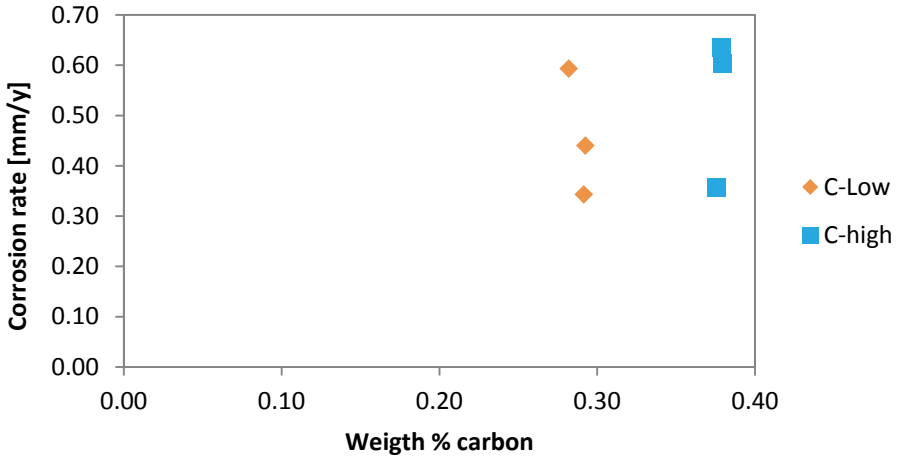

Figure 31 – Corrosion rate of J55 samples as a function of carbon content. Similar result was shown for all other elements, as no apparent trend could be demonstrated.

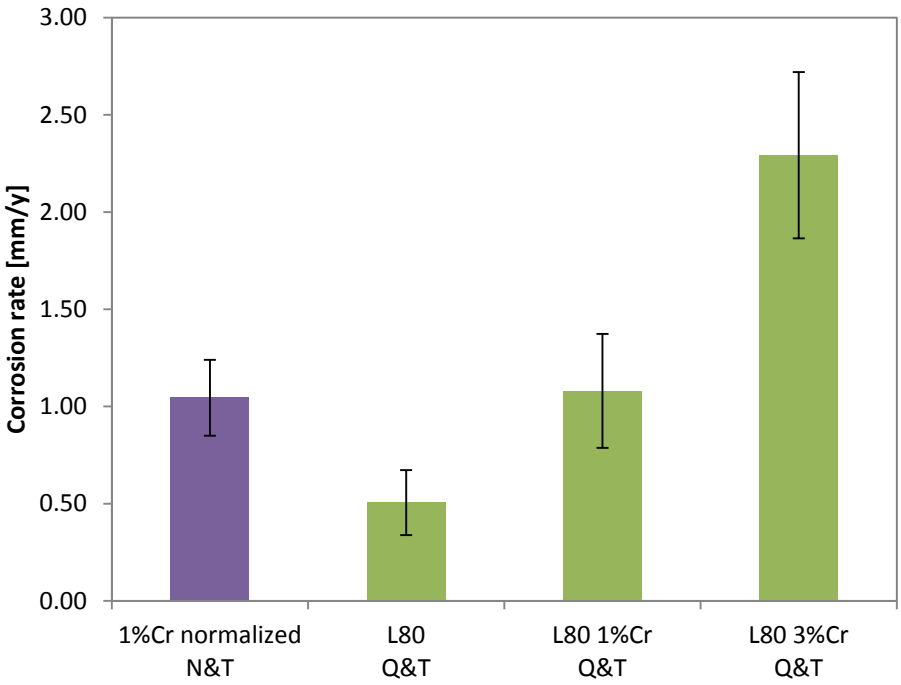

Figure 32 – Corrosion rate of J55 steel grades plus 1%Cr normalized proprietary grade. Parameters were 80°C, 26 bar CO_2 initial filling pressure, 5% NaCl and 5 days of exposure. Bars represent standard error.

Figure 32 shows the corrosion rate of L80 grades as well as the 1%Cr normalized proprietary grade. The chemical composition of the L80 grades is shown in Table 3. The compositions of this group show bigger differences with respect to alloying elements than the J55 grades, like the chromium content ranging from 0.055 to 3.095 wt-% or the carbon content raising from 0.086 to 0.37 wt-%. It is further notable, that sulfur was only found in traces and out of the working range.

Out of all chemical elements that were plotted against the corrosion rate, only chromium, manganese, molybdenum and copper showed a trend with a R^2 higher than 0.78. The predominant question is if all those elements influence the corrosion rate, or if chromium, which has an R^2 of 0.9993, is the main reason for the increased corrosion rate (Figure 33).

As manganese is an inexpensive alloying element compared to chromium or nickel, and it has beneficial effects for mechanical properties, it is often used instead of Cr and Ni. Therefore it is common that steel grades like sample “L80”, which have low amounts of Cr and Ni have higher amounts of Mn and vice versa for sample “L80 3%Cr”.

For the C1020 grades it will be shown below that Cu and Mo tend to decrease the corrosion rate. It is therefore rather unlikely that the same element increases the corrosion rate for one steel, and decreases it for another one. It is more plausible that Cr is responsible for the increased corrosion rate, and the other elements are only used as alloying elements and show this correlation by chance.

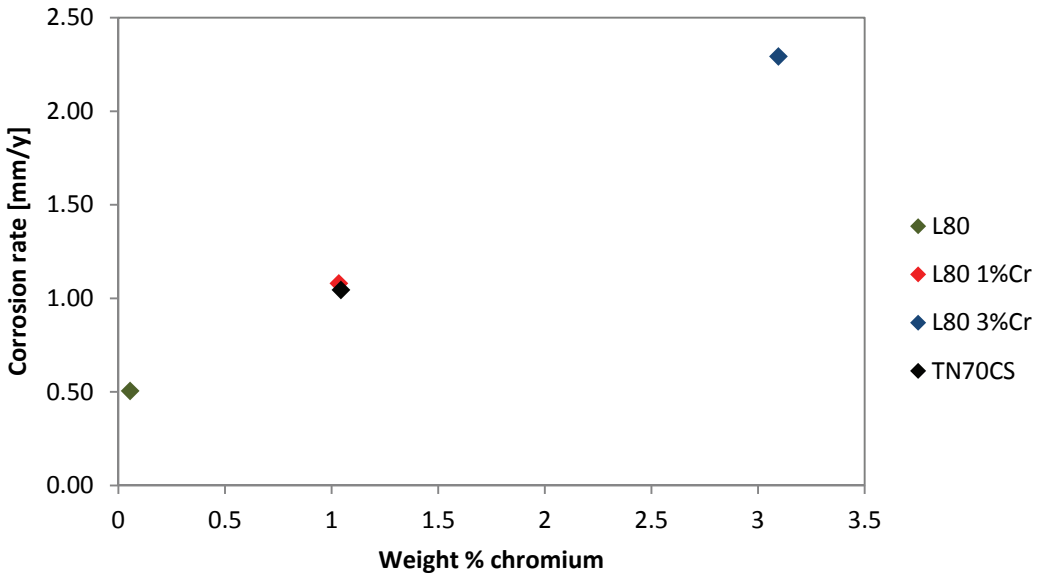

Figure 33 – Corrosion rate of L80 grades as a function of chromium content. Data taken from third experiment. R^2 calculated to be 0.9993.

C1020 grades

The difference between the old and the new batch of the C1020 standard coupons is low for most elements. Still, there are some elements with a difference which could lead to the different corrosion rates which were found. The amount of C, Mn, P, Ni, V, W, Ti, B and Nb was almost the same for both grades. Table 6 shows the different proportions of the remaining elements.

Table 6 – Corrosion rates and differences in chemical composition of both C1020 grades.

Grade	CR [mm/y]	S %	Cr %	Mo %	Cu %	Si %	Al %
C1020 new	0.43	0.00192	0.097	0.008	0.102	0.09117	0.023
C1020 old	1.22	0.01131	0.032	0.004	0.049	0.01099	0.051

The C1020 new grade has three times as much chromium, but still a lower corrosion rate of 0.43 mm/y compared to the 1.22 mm/y by the old grade. Two theories were established to explain why the corrosion rate is lower:

1. the effect of increased corrosion rate with increased amounts of chromium starts after a certain threshold, which is apparently higher than the 0.1 wt-% as in the new grade;
2. the effect of other chemical elements is higher and the influence of Cr cannot be seen.

The amount of sulfur in the old grade is almost six times as high as in the new grade. Since sulfur forms MnS very easily and is never found interstitial if enough Mn is prevalent, more MnS exists in the old grade. It is possible that due to the corrosion, the MnS inclusions detach from

the matrix, leaving pits. These pits can be used by the corrosive agents for enhanced corrosive attacks.

It was shown by Stegmann et al. [8] that the corrosion rate decreases, as silicon promotes a protective layer. As the wt-% of silicon is almost nine times as high for the new batch, a difference in its protection is possible.

4.2.2 Analysis of microstructure

It is of foremost importance to state, that the microstructure of a sample, and therefore the phases to be seen, are dependent on the chemical composition and thermo-mechanical history. A carbon content of 0.3 – 0.4 wt-%, which all J55 samples have, indicates that a ferritic/pearlitic (F/P) structure can be expected. As stated above, the final microstructure is not solely dependent on the carbon content, so the samples with different heat treatments show different structures. The following microstructures for J55 grades exist (Figure 34):

- homogenous F/P in the as rolled samples;
- band-type F/P in the twice normalized samples;
- tempered bainite in the quenched and tempered samples.

Various microstructures are present in the L80 and Cr containing grades (Figure 35):

- fine pearlite with small amounts of ferrite on the grain boundaries for 1%Cr normalized N&T;
- coarse tempered martensite for L80 Q&T;
- fine tempered martensite for L80 1%Cr Q&T;
- tempered martensite with retained austenite grain boarders for L80 3%Cr Q&T.

A mainly ferritic structure is present at the C1020 samples, with deformed grains due to the mechanical history and no performed heat treatment (Figure 36).

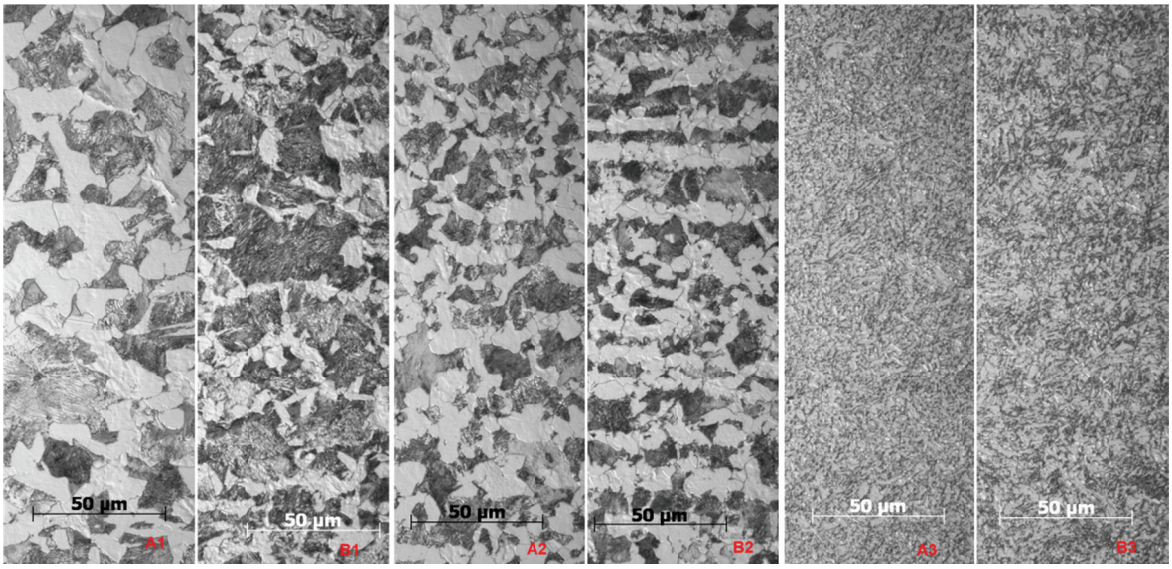

J55 C-high AR | J55 C-low AR | J55 C-high 2xN | J55 C-low 2xN | J55 C-high Q&T | J55 C-low Q&T

Figure 34 – From left to right, all 500x magnified: C-high as rolled, ferrite/pearlite; C-low as rolled, ferrite/pearlite; C-high 2xN, banded ferrite/pearlite; C-low 2xN, banded ferrite/pearlite; C-high Q&T, tempered bainite; C-low Q&T, tempered bainite.

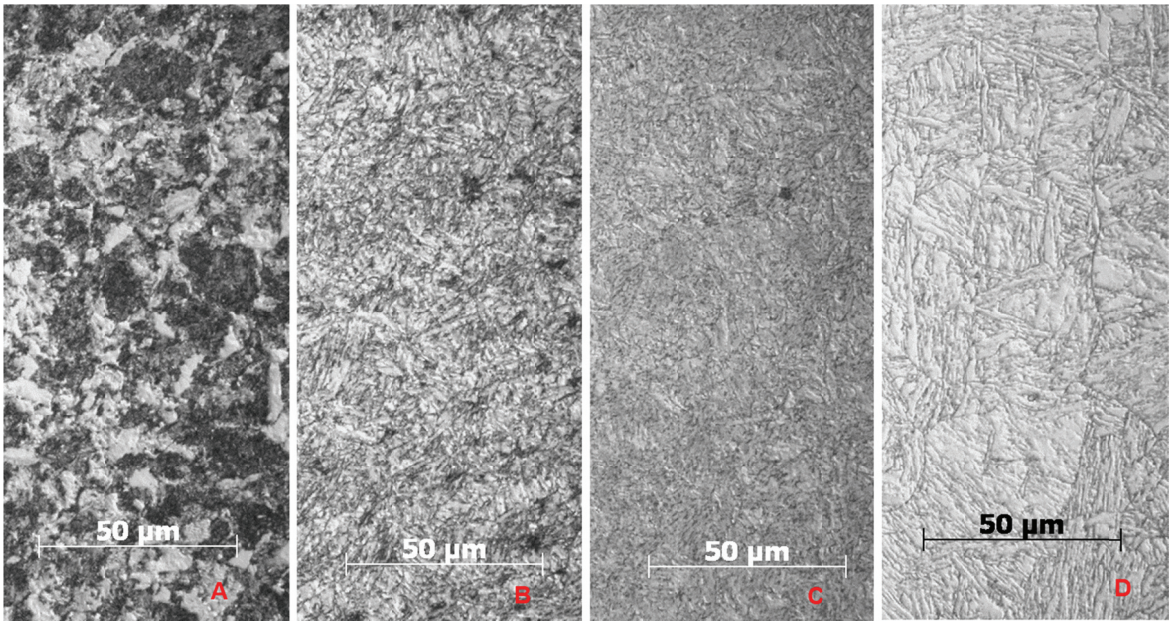

1%Cr normalized N&T | L80 Q&T | L80 1%Cr Q&T | L80 3%Cr Q&T

Figure 35 – From left to right, all 500x magnified: 1%Cr normalized N&T, L80 Q&T, L80 1%Cr Q&T, L80 3%Cr Q&T

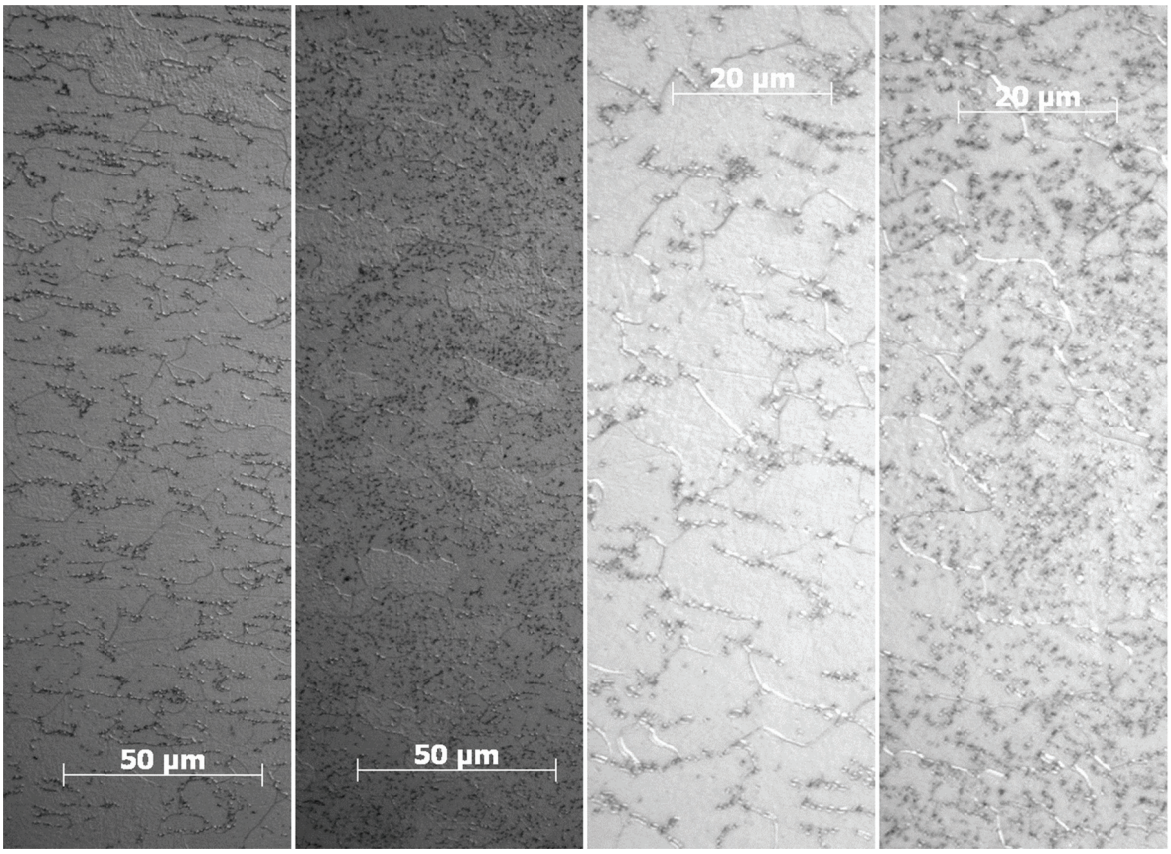

C1020 old batch, x500 C1020 new batch, x500 C1020 old batch, x1000 C1020 new batch, x1000

Figure 36 – C1020 grades. From left to right: 500x old batch, 500x new batch, 1000x old batch, 1000x new batch

The microstructure of both C1020 batches shows no variation (Figure 36). The microstructure appears ferritic and free from pearlite.

Figure 37 shows the corrosion rates of the microstructures of the J55 steel grades: the first bar represents the as rolled qualities. The grains are homogenously distributed through the sample and a little coarser than the twice normalized samples. The second bar represents the twice normalized samples, which have a finer grain size (Table 8) and a band-type formation. The third bar represents the quenched and tempered samples with their tempered bainitic microstructure.

The corrosion rate of the Q&T samples is about half as high as the corrosion rate of the AR samples, and still significantly smaller than the 2xN corrosion rate. It appears that the tempered bainitic microstructure has beneficial effects on the corrosion rate. Due to the large scatter band of the AR samples, no significant difference between the first two bars could be found with the student's t-test.

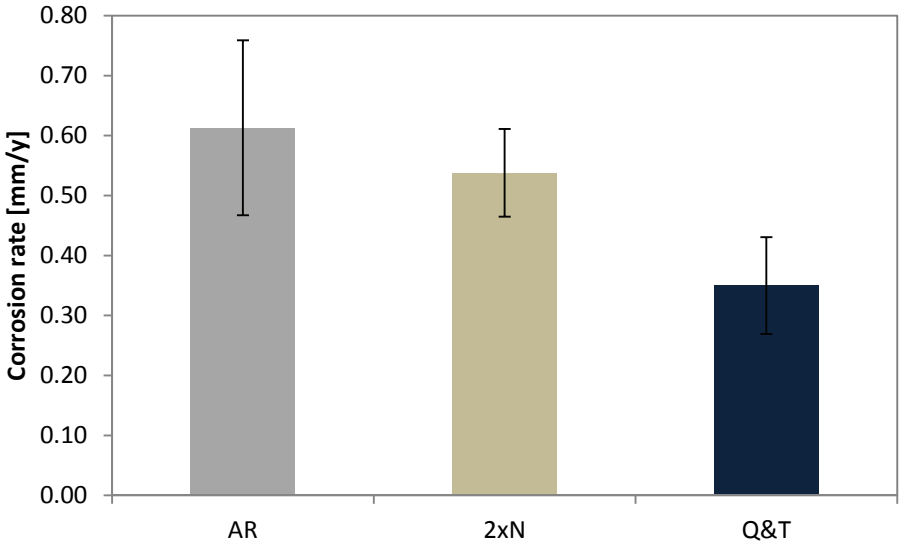

Figure 37 – Corrosion rate of the various microstructures of the J55 steel grade. Data taken from third experiment.

When comparing the structures of the J55 C-high grades to that of the J55 C-low grades (Figure 34, A1 and A2), the difference in the amount of existent pearlite can easily be seen. Although the C-low grade has less carbon content, the microstructure contains more pearlite phase, than the C-high grade. According to "De Ferri Metallographia" [57] manganese has the effect of stabilizing the pearlite phase. As Table 7 shows, there is more manganese present in the C-low quality than in the C-high.

Table 7 – Elements mainly responsible for formation of pearlite phase in the samples. Approximate percentage of pearlite phase in samples, determined with graphics program (Paint.NET) using area selection and pixel metering.

Grade	CR [mm/y]	Number	Heat Treatment	C %	Mn %	Pearlite %
J55 C-high	0.63	15	as rolled	0.38	0.65	~ 50
J55 C-high	0.64	24	2 x N	0.38	0.66	~ 40
J55 C-low	0.59	12	as rolled	0.28	1.40	~ 70
J55 C-low	0.44	18	2 x N	0.29	1.39	~ 50

For both heat treatments, the as rolled samples contained more pearlite than the twice normalized ones. With the high cooling speed of the as rolled samples, it was not possible for the microstructures to attain their ideal positions. An indicator for this is the somewhat acicular grain shape compared to the rather round grain shape of the twice normalized samples. Upon normalizing the steel twice, enough energy was inserted to form a more stable microstructure and the carbon had enough time to move to its preferred locations. As a consequence, less pearlite was present for the formation of pearlite.

No apparent influence of the amount of pearlite phase on the corrosion rate of the tested C-Steels can be seen (Figure 38). A decreased corrosion rate can be seen for the C-low samples with decreased pearlite phase, however as this behavior does not appear for the C-high samples, it is rather unlikely that the reduced corrosion rate is a consequence of the amount of pearlite phase.

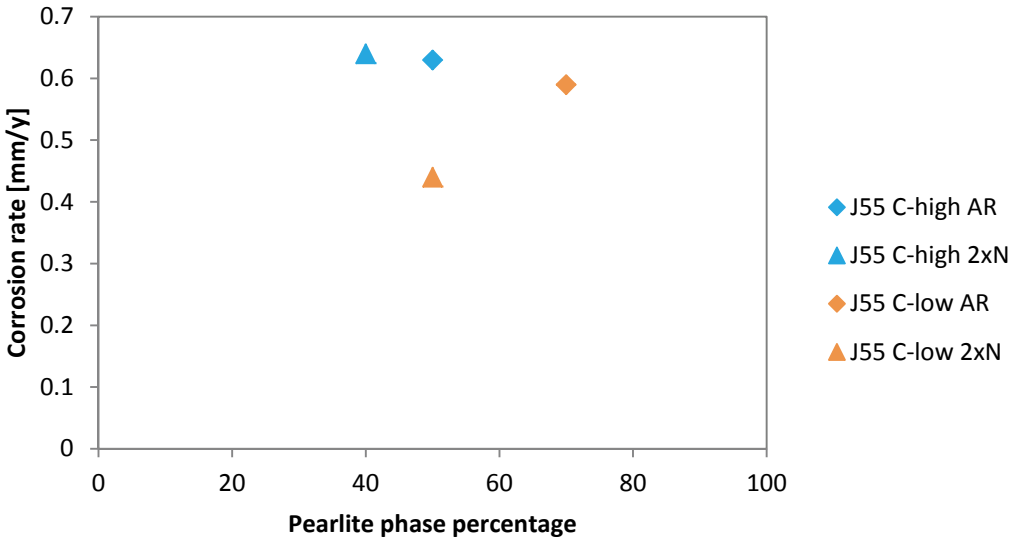

Figure 38 – Corrosion rate as a function of pearlite phase percentage. Data taken from third experiment.

The band type microstructure occurs because of the thermo-mechanical history of the tubings, which orientates the grains. Where the as rolled samples show no band type structure, the normalized samples have one. The as rolled tubings cool down at room temperature, thus the microstructure has not enough time to orientate the way it wants to. Grain movement is a diffusion controlled process, which is highly temperature dependent. When normalizing the tubings, enough energy in form of heat is inserted into them, activating the diffusion processes which are responsible for restructuring the grains. Hence the microstructure becomes banded.

4.2.3 Analysis of grain size

The grain size was measured with “Grain Size Charts” according to DIN 50601 [58] (Table 8).

Table 8 – Grain size measured using DIN 50601 grain size chart; TM – tempered martensite, TB – tempered Bainite, FP – ferrite/pearlite, F – ferrite. Homogeneity refers to evenly built grains or rather showing some other phenomenon. No grain size can be determined for TM or TB grains. CR: corrosion rate.

Grade	Number	Heat Treatment	Phases	Homogeneity	Grain Size	CR [mm/y]
L80	6	Q&T	TM	Y	--	0.51
L80 1%Cr	3	Q&T	TM	Y	--	1.08
L80 3%Cr	26	Q&T	TM	Y	--	2.29
1%Cr norm.	1	N&T	FP	Y	8 - 9	1.04
J55 C-high	15	As rolled	FP	Y	7 - 8	0.63
J55 C-high	24	2 x N	FP	banded	8 - 9	0.64
J55 C-high	31	Q&T	TB	Y	--	0.36
J55 C-low	12	As rolled	FP	Y	6 - 7	0.59
J55 C-low	18	2 x N	FP	banded	9 - 10	0.44
J55 C-low	32	Q&T	TB	Y	--	0.34
C1020 old	--	As rolled	F	Y	7 - 8	1.22
C1020 new	--	As rolled	F	Y	7 - 8	0.43

The influence of the grain size on the corrosion rate can be seen in Figure 39. This diagram was plotted with no respect to the difference in chemical composition. Only the grain size was used as a parameter. No trend can be seen.

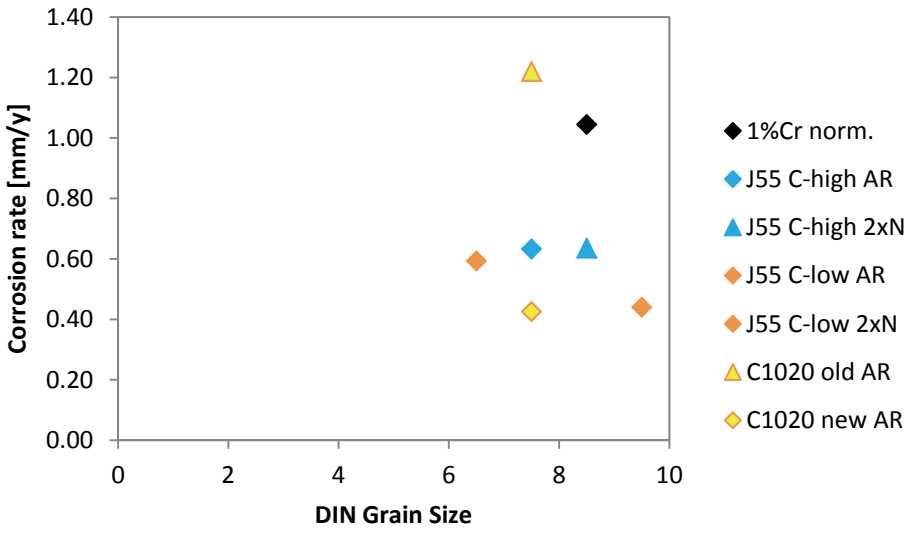

Figure 39 – Corrosion rate as a function of grain size. Data taken from third experiment.

5 Discussion

5.1 Effect of temperature

The result from the performed experiments (Figure 24) coincides well with literature [13; 29]. Although different authors present different temperatures for the maximum corrosion rate, the peak always exists between 60°C and 100°C. The shift in the peak can be explained with a different partial pressure [14]. An effect of flow or salinity should not be neglected as it was shown to have an impact on the corrosion rate [13; 31]; however, its influence on the peak is not known.

The peak itself can be explained by two contrary processes:

1. The corrosion rate increases with temperature, as the higher temperature causes increased diffusion and reaction speeds, and thus higher corrosion rates [4].
2. A higher temperature lowers the solubility of $FeCO_3$ in the brine and increases the thickness and overall protection of the scale [9].

For low temperatures, the corrosion rate keeps increasing, as long as the first process is predominant. At the peak, both processes are at equilibrium. Finally the second one predominates for higher temperatures.

5.2 Effect of CO_2 partial pressure

The data obtained by our experiments show that there is a lower corrosion rate at a partial pressure of 1 bar compared to the other pressures (Figure 25). Even though the corrosion rate decreases at the higher values, according to a performed t-Test it is not possible to differentiate any of the values, except the first one. The result is reasonable, when keeping the minor change of pH in the range of 5 to 50 bar (Figure 3) in mind.

A high influence of the CO_2 partial pressure seems to exist in the range from 0.1 to 3 bar, as shown by Nesic et al. [18]. This is plausible since the change in pH is huge, as shown in Figure 2. Although only calculated, this figure does not contradict our findings, as no tests were performed in this range. The results of Hesjevik et al. [21] show that at very high pressures the corrosion rate decreases again. A curve similar to the one of temperature is likely, but was not measured yet. No single test was performed over the full range of pressures, from very low to very low, in order to chart the pressures influence on the corrosion rate.

5.3 Effect of the amount of medium used

The “half-side-corrosion” effect observed in our experiments can be compared to the increased corrosion rate of pipes at the six o’clock position [59; 60]. The increased corrosion rate can come

from the fact, that the upper part of the coupon is only wetted periodically. This wet film can saturate with Fe^{2+} ions much faster, than the bulk can, which would promote the formation of a scale. The lower part which is continuously wetted is permanently in contact with the medium, hence corrosive species as well as corrosion products can diffuse to and from the surface at any time. The permanently wetted part showed increased localized corrosion, which was also reported by Sydberger [59].

In order to decrease the variance and achieve more concise results, the amount of medium was decreased from 80ml to 50ml. With this decrease, the localized corrosion effect on the lower half of the coupons was eliminated, and hence the variance decreased.

5.4 Final pressure after autoclave testing

The fit in Figure 28 shows a good correlation between the mass loss of the coupons per autoclave and the measured final pressure. When using the ideal gas equation and the given data, a similar mass loss can be calculated.

Combining Figure 28 and Table 5, the postulated theory two seems to be correct. Theory two said, that the pressure in the autoclaves increases, as the corrosion rate increases, due to the evolution of H_2, which cannot dissolve in the medium.

5.5 Effect of chemical composition

As shown in chapter 4.2.1, our experiments show an unfavorable effect of chromium upon alloying. This is in contrast with most of the literature referenced in 2.2.1. The main differences between the tests performed by other authors and this one are the ratio of volume of medium and surface area, as well as flow parameters and pressure.

Most of the authors which report beneficial effects of chromium performed their experiments at partial pressures of 1-2 bar [25; 26; 27; 28; 29; 30]. At higher partial pressures, the effect of chromium seems to diminish [13; 33; 35]. This is in good correlation with our results as a pressure of 26 bar was used.

According to Muraki et al. [28] the corrosion rate of chromium steels is intrinsically higher than of carbon steels. After some time, a chromium layer forms which offers protection. However when combining this result with the very low medium to surface ratio, another effect could be seen: The medium saturates very quickly and a protective carbonate layer is formed. This happens on the carbon steel as well as on the chromium steel. Up to the point where the protective layer is formed, the chromium steel shows higher corrosion rates.

For high chloride concentrations of 30000ppm it was shown by Ikeda et al. [13] in Figure 8 that the corrosion rate of a 2.0% chromium steel is higher than the 0.5% chromium steel after 100 hours. This result fits our results very well, as the same salinity and exposure time was used.

Figure 7 shows the effect of temperature on the corrosion rate of various Cr steel grades. The figure shows that at 100°C the corrosion rate of low alloyed steel grades is higher than for 0% chromium. At 80°C however this figure shows a beneficial effect of chromium. Taking the findings of Dugstad et al. [31] into account, which showed that for slow flow velocities of 0.1 m/s chromium offered no longer beneficial effects, it is questionable, whether the peaks of Figure 7 are set in stone, or if they are dependent on flow and other parameters. It is important to mention that the 0% chromium peak of Figure 7 is located at a higher temperature than measured in Figure 24, thus a shift of all peaks to a lower temperature could be possible.

Without any doubt, there are certain parameters, at which chromium has proven its value in the protection of steel; however for the above stated reasons, at the used parameters in this experiment, chromium showed detrimental results.

5.6 Effect of microstructure

In our experiments, the lowest and the highest corrosion rates were achieved by a quenched and tempered microstructure (Figure 29). However, when grouping the steel grades into unalloyed and low alloyed grades, the high corrosion rates can easily be explained by the influence of chromium. Figure 37 shows that in the experiments performed, the quenched and tempered microstructure of the J55 grades shows the smallest corrosion rate. This result coincides with some authors of the literature [8; 37; 40]. Paolinelli et al. [42] explained the beneficial effect of the tempered martensitic structure due to the globular cementite phase within the ferrites matrix. As the ferrite corrodes away, the cementite detaches, and the cathodic surface area stays relatively constant. For the ferritic pearlitic structure however, the cementite network stays, as the ferrite corrodes away, thus the cathodic surface increases, which leads to an increased corrosion rate.

Still, there are many other authors, reporting a beneficial effect for the ferritic pearlitic structure [11; 39; 40; 41] and all of their presented theories, presented in 2.3, seem to be plausible.

There definitely is an effect of the microstructure on the corrosion rate; however, it is not known how big of an impact this influence is.

5.7 Effect of grain size

Neither the grain size, nor the band-type structure, seemed to have a large impact on the corrosion rates in the tests performed. A special investigation in this topic could reveal some information, however the differences in grain size were either too small to measure different

corrosion rates, or the influence of the grain size on the corrosion rate is so low that it is overshadowed by other parameters such as chemical composition.

To obtain a clear conclusion, it would be necessary to examine the exact same steel, with different grain sizes.

5.8 Validity of predictive CO_2 corrosion models

When applying all necessary factors to the deWaard-Milliams equation, the calculated corrosion rate for the parameters used in our test is about a factor 10 higher than the observed one.

The problem when using the NORSOK model with the parameters of our experiments is the upper limit of the fugacity of CO_2 of 10 bar. When calculating with less pressure, the actual corrosion rate will be underestimated. Still, the corrosion rate calculated is almost twice as high as the corrosion rate calculated using the deWaard-Milliams equation.

As we experience scale formation, it is not possible to use the models of Nesic et al. or Mishra et al. Their models are based upon chemical reaction-controlled processes which change to diffusion controlled after the formation of scales [18; 19]. The authors of the NORSOK formula also indicated that corrosion rates can differ greatly if scale formation is experienced, and it has to be included in the calculations [20]. DeWaard et al. used a scaling factor to account for the appearance of the scale. However, the formula in the nomogram seems to be too conservative as the corrosion rate is still more than 10 times higher than the one measured in our experiments. In their publication, they show a compilation of scale factors of other authors together with theirs. The figure shows that the corrosion rate can change by a factor 10, simply by using the scaling factors of other authors.

The models couldn't be used in the experiments conducted because scale formation was observed in every case. The calculated corrosion rates were an order of magnitude higher and the parameters used in the experiments were outside of the boundaries of most models. Depending on how much conservatism is built into the model and which parameters are taken into account, the models can give a difference up to two decades [3].

5.9 Comparison between autoclave and electrochemical tests

The determination of corrosion rates by the use of electrochemical tests has been applied by many authors, who found a relationship between the corrosion current density and the corrosion rate. Those authors also developed models, to predict the corrosion rate from knowing only a few parameters.

However, such measurements are only satisfyingly correct, if the measured curve can be fit by unique tangents, as shown in Figure 21. If the curve looks more like Figure 22, where no unique tangent can be found, the resulting corrosion rate lies between an order of magnitude.

Another concern is the formation of a layer, which changes the corrosion rate and behavior drastically. Many models fail at the point, where film formation begins.

All the measured steel samples showed a small deviation from each other. No correlation between the corrosion rates of the autoclave tests and the electrochemical tests were found. The differences in the steel grades, seemed to be too small, to have an influence on the measured curve. However the impact on the corrosion rates in the autoclave tests was immense.

It was shown, that the linear polarization method, which was used in the experiments, is not capable of predicting the exact corrosion rate for the chosen system and parameters. This was already stated by Schmitt et al. [34] who wrote that practically relevant conclusions can only be obtained by direct weight loss measurements.

6 Conclusion

The output of this master thesis is, that the determination and prediction of the corrosion rate of un- and low-alloyed steel grades, is dependent on a great number of parameters. The corrosion rate seems to be a function of system parameters, like temperature, pressure, exposure time, salinity, etc., and metallurgical parameters such as chemical composition, microstructure, thermomechanical history, etc.

It was the authors concern, that most of these parameters were investigated, either by the means of literature review, conducting experiments or both. The findings are presented in the previous chapters.

The final results, shown in Figure 29, are only a section of the corrosive behavior of the tested steels, as no change in the parameters was conducted. In order to achieve a full answer, a variation in temperature, pressure, and other parameters, resulting in a huge testing matrix, would be necessary.

For the given information of the literature review, and the measured results of the experiments, the most corrosion resistant steel grades, are quenched and tempered J55 grades, with no chromium. The highest corrosion rate was measured on a L80 grade with 3% chromium, followed by two different steel grades with each 1% chromium.

The biggest impact on the corrosion rate was delivered by chromium, shown in Figure 33. The influence of the microstructure, measured on J55 grades, was not as conclusive, due to the large standard error. Still, the quenched and tempered samples seem to perform better than the other heat treatments (Figure 37).

No influence of the band type structure, the amount of pearlite phase (Figure 38), or the grain size (Figure 39) on the corrosion rate could be measured.

An evaluation of various CO_2 corrosion models, showed that all of them are too conservative in overestimating the corrosion rate. Some of them even fail and cannot be used anymore, as scale formation begins.

In the end, this master thesis has to be seen as a piece in the puzzle, which describes the CO_2 corrosion and its influences. More work on the influences of the above listed parameters has to be done.

7 References

[1] J.L. Crolet, Which CO_2 Corrosion, Hence Which Prediction?, European Federation of Corrosion #13: Predicting CO_2 Corrosion in the Oil and Gas Industry, 1994, 1-29.

[2] P.W. Atkins, Physikalische Chemie, 2te Auflage, VCH Verlagsgesellschaft, Weinheim, Germany, 1996, 205.

[3] A. Dugstad, Fundamental Aspects of CO_2 Metal Loss Corrosion - Part I: Mechanism, CORROSION 2006, paper no. 06111, Houston, TX: NACE International, 2006.

[4] C. deWaard, D.E. Milliams, Carbonic Acid Corrosion of Steel, Corrosion 31 (1975) 177-181.

[5] G.I. Ogundele, W.E. White, Some observations on Corrosion of Carbon Steel in Aqueous Environements Containing Carbon Dioxide, Corrosion 42 (1986) 71-78.

[6] D.G. Li, Y.R. Feng, Z.Q. Bai, M.S. Zheng, Characteristics of CO_2 corrosion scale formed on N80 steel in stratum water with saturated CO_2, Applied Surface Science 253 (2007) 8371-8376.

[7] C. deWaard, U. Lotz, Prediction of CO_2 Corrosion of Carbon Steel, European Federation of Corrosion #13: Predicting CO_2 Corrosion in the Oil and Gas Industry, 1994, 30-49.

[8] D. Stegmann, R. Hausler, C. Cruz, Laboratory Studies on Flow Induced Localized Corrosion in CO_2/H_2S Environments, I. Development of Test Methodology, CORROSION 90, paper no. 15, Houston, TX: NACE International, 1990.

[9] K. Videm, A. Dugstad, Corrosion of Carbon Steel in an Aqueous Carbon Dioxide Environment - Part 2: Film Formation, Material Performance (1989) 46-50.

[10] J.L. Crolet, N. Thevenot, S. Nesic, Role of Conductive Corrosion Products in the Protectiveness of Corrosion Layers, Corrosion 54 (1998) 194-203.

[11] C.A. Palacios, J.R. Shadley, Characteristics of Corrosion Scales on Steels in a CO_2-Saturated NaCl Brine, Corrosion 47 (1991) 122-127.

[12] G. Schmitt, M. Hörstemeier, Fundamental Aspects of CO_2 Metal Loss Corrosion - Part II: Influence of Different Parameters on CO_2 Corrosion Mechanism, CORROSION 2006, paper no. 06112, Houston, TX: NACE International, 2006.

[13] A. Ikeda, M. Ueda, CO_2 Corrosion Behaviour of Cr-containing Steels, European Federation of Corrosion #13: Predicting CO_2 Corrosion in the Oil and Gas Industry, 1994, 59-93.

[14] C. deWaard, U. Lotz, D.E. Milliams, Predictive Model for CO2 Corrosion Engineering in Wet Natural Gas Pipelines, Corrosion 47 (1991) 976-985.

[15] M.B. Kermani, A. Morshed, Carbon Dioxide Corrosion in Oil and Gas Production - A Compendium, Corrosion 59 (2003) 659-683.

[16] K. Videm, A. Dugstad, Corrosion of Carbon Steel in an Aqueous Carbon Dioxide Environment - Part 1: Solution Effects, Material Performance (1989) 63-67.

[17] Z. Duan, R. Sun, An improved model calculating CO_2 solubility in pure water and aqueous NaCl solutions from 273 to 533 K and from 0 to 2000 bar, Chemical Geology 193 (2003) 257-271.

[18] S. Nesic, J. Postlethwaite, S. Olsen, An Electrochemical Model for Prediction of Corrosion of Mild Steel in Aqueous Carbon Dioxide Solutions, Corrosion 52 (1996) 280-294.

[19] B. Mishra, S. Al-Hassan, D.L. Olson, M.M. Salama, Development of a Predictive Model for Activation-Controlled Corrosion of Steel in Solution Containing Carbon Dioxide, Corrosion 53 (1997) 852-859.

[20] NORSOK Standard, M-506: CO_2 corrosion rate calculation model. June 2005, Rev. 2.

[21] S. M. Hesjevik, S. Olsen, M. Seiersten, Corrosion at High CO_2 Pressure, CORROSION 2003, paper no. 03345, Houston, TX: NACE International, 2003.

[22] M. Seiersten, Material Selection for Separation, Transportation and Disposal of CO_2, CORROSION 2001, paper no. 01042, Houston, TX: NACE International, 2001.

[23] S. Nesic, L. Lunde, Carbon Dioxide Corrosion of Carbon Steel in Two-Phase Flow, Corrosion 50 (1994) 717-728.

[24] Z.F. Yin, Y.R. Feng, W.Z. Zhao, Z.Q. Bai, G.F. Lin, Effect of temperature on CO_2 corrosion of carbon steel, Surface and Interface Analysis 41 (2009) 517-523.

[25] U. Lotz, T.Sydberger, CO_2 Corrosion of Carbon Steel and 13Cr Steel in Particle-Laden Fluid, Corrosion 44 (1988) 800-809.

[26] A. Pfennig, R. Bäßler, Effect of CO_2 on the stability of steels with 1% and 13% Cr in saline water, Corrosion Science 51 (2009) 931-940.

[27] M.B. Kermani, J.C. Gonzales, G.L. Turconi, D. Edmonds, G. Dicken, L. Scoppio, Development of Superior Corrosion Resistance 3%Cr Steels for Downhole Applications, CORROSION 2003, paper no. 03116, Houston, TX: NACE International.

[28] T. Muraki, K. Nose, H. Asahi, Development of 3% chromium linepipe steel, CORROSION 2003, paper no. 03117, Houston, TX: NACE International, 2003.

[29] H. Inaba, M. Kimura, H. Yokokawa, An Analysis of the Corrosion Resistance of Low Chromium-Steel in a Wet CO_2 Environment by the Use of an Electrochemical Potential Diagram, Corrosion Science 38 (1996) 1449-1461.

[30] D.S. Carvalho, C.J.B. Joia, O.R. Mattos, Corrosion rate of iron and iron-chromium alloys in CO_2 medium, Corrosion Science 47 (2005) 2974-2986.

[31] A. Dugstad, L. Lunde, K. Videm, Influence of alloying elements upon the CO_2 corrosion rate of low alloyed carbon steels, CORROSION 1991, paper no. 473, Houston, TX: NACE International, 1991.

[32] D. Edmonds, R. Cochrane, The effect of alloying on the resistance of carbon steel for oilfield applications to CO2 corrosion, 59th Annual Congress of ABM - International, Sao Paulo, Brazil: ABM, 2004, 4770-4784.

[33] M. Oberndorfer, K. Thayer, Development of New Steel Qualities for the Oil and Gas Production, Vienna, Internal OMV Report, 1999.

[34] G. Schmitt, B. Rothmann, Corrosion of Unalloyed and Low Alloyed Steels in Carbonic Acid Solutions, Werkstoffe und Korrosion 29 (1978) 237ff.

[35] C. Bosch, J.P. Jansen, R.K. Poepperling, Influence of chromium contents of 0.5% to 1.0% on the corrosion behavior of low alloy steel for large-diameter pipes in CO_2 containing aqueous media, CORROSION 2003, paper no. 03118, Houston, TX: NACE International, 2003.

[36] J. Guo, S. Yang, C. Shang, Y. Wang, X. He, Influence of carbon content and microstructure on the corrosion behavior of low alloy steels in a Cl- containing environment, Corrosion Science 51 (2008) 242-251.

[37] S. Al-Hassan, B. Mishra, D.L. Olsen, M.M. Salama, Effect of Microstructure on Corrosion of Steels in Aqueous Solutions Containing Carbon Dioxide, Corrosion 54 (1998) 480-491.

[38] D.A. Lopez, W.H. Schreiner, S.R. de Sanchez, S.N. Simison, The influence of carbon steel microstructure on corrosion layers - An XPS and SEM characterization, Applied Surface Science 207 (2003) 69-85.

[39] D. Clover, B. Kinsella, B. Pejcic, R. de Marco, The influence of microstructure on the corrosion rate of various carbon steels, Journal of Applied Electrochemistry 35 (2005) 139-149.

[40] B. Mishra, S. Al-Hassan, D.L. Olson, M.M. Salama, Prediction of Microstructural Effect on Corrosion of Linepipe Steels in CO_2-Brine Solution, CORROSION 1993, paper no. 90, Houston, TX: NACE International, 1993.

[41] G. Chitwood, W. Coyle, R. Hilts, A case-history analysis of using plain carbon & alloy steel for completion equipment in CO_2 service, CORROSION 1994, paper no. 20, Houston, TX: NACE International, 1994.

[42] L.D. Paolinelli, T. Perez, S.N. Simison, The effect of pre-corrosion and steel microstructure on inhibitor performance in CO_2 corrosion, Corrosion Science 50 (2008) 2456-2464.

[43] D.A. Lopez, S.N. Simison, S.R. de Sanchez, The influence of steel microstructure on CO_2 corrosion - EIS studies on the inhibition efficiency of benzimidazole, Electrochimica Acta 48 (2003) 845-854.

[44] D.A. Lopez, S.N. Simison, S.R. de Sanchez, Inhibitor performance in CO_2 corrosion - EIS studies on the interaction between their molecular structure and steel microstructure. Corrosion Science 47 (2005) 735-755.

[45] C. Vega, N. Ochoa, N. Pebere, J. Lacaze, J.L. Brito, An investigation on CO_2 corrosion resistance of carbon steel in relation with microstructural changes, 216th ECS Meeting, abstract no. 1692, Pennington, NJ: ECS, 2009.

[46] L.D. Piper, W.D. McCain Jr., J.H. Corredor, Compressibility Factors for Naturally Occurring Petroleum Gases, SPE 26668, 1993.

[47] DIN 53804-1:2002-04 - Ausreißertest nach Dixon.

[48] ASM International, J.R. Davis, Corrosion - Understanding the basics, ASM International, Materials Park, OH, USA, 2000, 458-461.

[49] H. Czichos, T. Saito, L. Smith, Handbook of Materials Measurement Methods, Springer Science+Business Media Inc., Leipzig, 2006, 644.

[50] R. Storm, Wahrscheinlichkeitsrechnung mathematische Statistik und statistische Qualitätskontrolle, VEB Fachbuchverlag Leipzig, Leipzig, 1976, 167.

[51] I.N. Bronstein, K.A. Semendjajew, Taschenbuch der Mathematik, Wissenschaftlicher Verlag Harri Deutsch GmbH, Frankfurt a. d. Main, 2008, 828.

[52] K. Gao, F. Yu, X. Pang, G. Zhang, L. Qiao, W. Chu, M. Lu, Mechanical properties of CO_2 corrosion product scales and their relationship to corrosion rates, Corrosion Science 50 (2008) 2796-2803.

[53] G. Lin, M. Zheng, Z. Bai, X. Zhao, Effect of Temperature and Pressure on the Morphology of Carbon Dioxide Corrosion Scales, Corrosion 62 (2006) 501-507.

[54] K. Sapre, S. Seal, P. Jepson, H.B. Wang, Z. Rahman, T. Smith, Investigation into the evolution of corrosion product layer (CPL) of 1018 C-steel exposed to multiphase environment using FIB and EIS techniques, Corrosion Science 45 (2003) 59-80.

[55] S.L. Wu, Z.D. Cui, F. He, Z.Q. Bai, S.L. Zhu, X.J. Yang, Characterization of the surface film formed from carbon dioxide corrosion on N80 steel, Material Letters 58 (2004) 1076-1081.

[56] J.L. Mora-Mendoza, S. Turgoose, Fe_3C influence on the corrosion rate of mild steel in aqueous CO_2 systems under turbulent flow conditions, Corrosion Science 44 (2002) 1223-1246.

[57] A. Schrader, A. Rose, De Ferri Metallographia, Verlag Stahleisen m.b.H., Düsseldorf, 1966, 80.

[58] DIN 50601, Seite 5, Bild 1 - Bildreihentafel zur Bestimmung der Korngröße.

[59] T. Sydberger, Flow dependent corrosion: mechanisms, damage characteristics, and control, British Corrosion Journal 22 (1987) 83-89.

[60] R. Duncan, Gathering Lines Corrosion in the Bahrain Crude Field, Materials Performance 12 (1983) 13-14.